Anionically-functionalized glycogen encapsulates melittin by multivalent interaction

Hanna Zhukouskaya[1], Pablo M. Blanco[2], Zulfiya Černochová[1], Lucie Čtveráčková[1], Roman Staňo[3], Ewa Pavlova[1], Miroslav Vetrík[1], Peter Černoch[1], Miroslav Šlouf[1], Marcela Filipová[1], Miroslav Štěpánek[2], Martin Hrubý[1], Peter Košovan[2*], Jiří Pánek[1*].

[1]Institute of Macromolecular Chemistry, Czech Academy of Sciences, Heyrovského nám. 2, 162 06 Prague 6, Czech Republic

[2]Department of Physical and Macromolecular Chemistry, Faculty of Science, Charles University, Hlavova 8, 128 40 Prague 2, Czech Republic

[3]Faculty of Physics, University of Vienna, Kolingasse 14-16, 1090 Vienna, Austria

e-mail: panek@imc.cas.cz peter.kosovan@natur.cuni.cz

Keywords: melittin, glycogen, polyelectrolyte, encapsulation, hemolysis, charge regulation

ABSTRACT

We developed acid-functionalized glycogen conjugates as supramolecular carriers for efficient encapsulation and inhibition of a model cationic peptide melittin - the main component of honeybee venom. For this purpose, we synthesized and characterized a set of glycogens, functionalized to various degrees by several different acid groups. These conjugates encapsulate melittin up to a certain threshold amount, beyond which they precipitate. Computer simulations showed that sufficiently functionalized conjugates electrostatically attract melittin, resulting in its efficient encapsulation in a broad pH range around the physiological pH. Hemolytic assays confirmed *in vitro* that the effective inhibition of melittin's hemolytic activity occurs for highly functionalized samples, whereas no inhibition is observed when using low-functionalized conjugates. It can be concluded that functional glycogens are promising carriers for cationic molecular cargos or antidotes against animal venoms under conditions, in which suitable properties such as biodegradability and biocompatibility are crucial.

INTRODUCTION

Nowadays, a number of naturally occurring and pharmacologically active substances of animal and plant origin draw attention as promising key components for novel drug formulations. Among the former, venoms of certain insects are of high interest due to their wide availability and yet unstudied clinical applications. An especially noteworthy example is melittin, a toxic peptide that constitutes approximately 50% of honeybee venom.[1] This substance has demonstrated anti-inflammatory,[2] anti-diabetic,[3] bactericidal,[4] and antiviral properties.[5] Moreover, melittin is a prominent candidate for cancer treatment, because it is able to suppress the development of drug resistance by cancer cells due to affecting the entire cell membrane structure rather than a specific cellular component.[6] Melittin is a linear, cationic, amphipathic, pore-forming peptide composed of 26 amino acid residues, whose sequence can be found in Fig. 1. The N- and C-terminal regions are mainly hydrophobic and hydrophilic, respectively.[7] The total net charge of melittin at physiological pH can be estimated from the Henderson-Hasselbalch equation to be +5, thus the peptide is attracted to negatively charged cell membrane surfaces, leading to the pore formation, followed by disruption of the integrity of phospholipid bilayers, which causes cell lysis and eventually leads to its death. This effect was observed in all prokaryotic and eukaryotic cell membranes and even in the case of artificial lipid membranes, therefore it is difficult to administer melittin *in vivo* due to its immediate action against the living cells. It can be considered as a venom diffusion factor, facilitating the entry of insect venom into the blood stream of stung victims. Lytic properties of this peptide also include strong hemolytic activity, governed by specific sequence of the N-terminal region, ability of peptide chain to reversibly change its conformation from helical to random coil, presence of charged amino acid residues, namely Lys and Arg, and especially important hydrophobic Trp residue at position 19, that binds to cholesterol present in cell membranes.[8,9] Because of its amphiphilic properties, melittin can be considered a surfactant; it activates phospholipase A2 enzyme and acts together with the enzyme as a direct hemolytic factor. Innate detergent-like effect of melittin affects red blood cells by lowering the surface tension of water at the level of plasma membrane, which leads to membrane disruption and cell lysis already at sub-micromolar concentrations of melittin. This process is referred to as hemolysis, *i.e.*, erythrocyte destruction[10] which results in the release of hemoglobin from erythrocytes to the surroundings.[11] At low concentrations melittin exists mostly in the unimeric form that has the conformation of a random coil. At higher concentrations, melittin molecules associate to tetramers, that do not cause hemolysis under identical conditions. Melittin tetramers have α-helical conformation where the active Trp19 fragment is sterically hindered. This association is also triggered by multivalent anions, such as phosphate, which therefore

suppress the hemolytic activity of melittin. However, it is possible to reverse the association by a temperature increase.[11,12] Therefore, an effective strategy for suppressing the hemolytic activity of melittin might consist in inducing its aggregation with multivalent anionic macromolecules.

Natural carbohydrate polymers, *i.e.*, polysaccharides, are promising candidates for this application, thanks to their non-toxicity, biocompatibility, biodegradability, and low cost of production as compared to synthetic biopolymers.[13] Other carrier-based delivery strategies have been developed to suppress the lytic properties of melittin before its release at the target destination. These include various polymeric nanoparticles,[14] poly(ethylene glycol)-stabilized lipid disks,[15] phospholipid monolayer-coated nanoemulsions,[16] as well as peptide hydrogels[17] and porphyrin compounds.[16] However, the advantage of using polysaccharides is that their abundant reactive hydroxyl group can be easily modified, which allows fine tuning of the response to various stimuli, for example pH. The latter allows to control the drug release by introducing both diagnostic and therapeutic entities in the resulting carrier.[18,19] Most studies of polysaccharide-based drug delivery systems describe derivatives or composites of chitosan,[20] alginate,[21] hyaluronic acid,[22] dextran,[23] or starch.[24] However, just a few sources mentioned the potential of glycogen for biomedical applications,[19] which is one of the most widely available carbohydrate polymers in nature. Glycogen is a spherical hyperbranched polysaccharide, tens-of-nanometers in size. It is highly biocompatible, completely biodegradable, soluble in water, abundant and easy to functionalize.[25,26] These properties make glycogen conjugates promising candidates for drug delivery and other pharmaceutical applications.[27]

The main idea of this study was to develop a novel concept of controlling encapsulation and release of model cationic peptide melittin by charge regulation and multivalent interactions with supramolecular polymer carriers based on anionically modified glycogens. We tested the idea simultaneously *in silico* and *in vitro*. For this purpose, we synthesized glycogen conjugates acylated with cyclic anhydrides of different acidity and hydrophobicity. In this way we produced biodegradable well-defined anionic encapsulators for melittin as a model cationic biomacromolecule. After the synthesis and characterization of the modified glycogens, we investigated their interactions with melittin by simultaneously following three different pathways: (1) Molecular simulations to understand the effect of the degree of substitution and solution pH on the interactions between modified glycogen and melittin; (2) Physico-chemical characterization of solutions containing modified glycogen and melittin at various concentration ratios and selected pH values; (3) *In vitro* hemolytic tests to determine the ability of selected modified glycogen samples to inhibit the hemolytic activity of melittin.

Thereby we present a unique full story of how a synergy between *in silico* simulations and *in vitro* chemistry allowed us to construct highly tunable supramolecular polymer carriers which work as encapsulators and scavengers of charged bioactive cargos, exploiting multivalent interactions. To the best of our knowledge, such a complex approach, resulting in a fully functional charge-regulating system, has not been reported in the literature. We focused on the pH values relevant for the intended application, ranging from 5 (late endosome after internalization into c ells) to 7.4 (blood plasma).[28] Our results show that such functional glycogen carriers are potentially suitable as controlled release carriers or antidotes against animal venoms, where widely adjustable properties, temperature-responsivity, biodegradability, and biocompatibility are crucial.

MATERIALS AND METHODS

Theoretical model

To understand the interaction between functionalized glycogen and melittin, we constructed a simplified simulation model. For brevity, we provide here a brief description of the model and refer to the supporting information (SI) for full technical details of the simulation. To represent the simulated molecules, bead-spring models are used where one spherical particle (bead) corresponds to one monomeric unit of the polymer. The beads are distinguished only by their acid-base properties, defined by the pKa value, protonation state, and their respective charge. The solvent is treated implicitly as a dielectric continuum; however, salt ions are treated as explicit particles. Such a simplified model accounts for steric repulsion, connectivity of the macromolecules, their conformational flexibility and electrostatic interactions. Our model neglects specific short-range interactions, such as hydrophobic interactions or hydrogen bonding. This last simplification was validated *a posteriori* by agreement between the trends observed in simulations and in experiments, suggesting that the neglected interactions are not dominant in the studied system. Similar coarse-grained models are ubiquitous in polymer science and have been used in our previous publications to model short peptides[29,30] or disordered proteins.[31]

The simulation box length was chosen such that one hyperbranched polymer in the simulation box corresponds to c_{glyc} = 1.5 mg/mL, assuming that one bead corresponds to one glucose unit of glycogen. Accordingly, 22 melittin molecules in the simulation box correspond to melittin concentration 1.42 mg/mL. Finally, 911 pairs of monovalent cations and anions have were added to obtain the salt concentration $c_{cat} = c_{an} = c_s$ = 20 mM. For simplicity, we will further refer to the monovalent ions as Na^+ and Cl^-.

The simulation was performed by combining the Langevin Dynamics to account for evolution of configurations, and a constant-pH Monte Carlo algorithm to account for acid-base equilibrium of all titratable groups. Further technical details of the simulation algorithm and simulation protocol are given in the Supporting Information.

Materials

Melittin from honeybee venom, anhydrides of *trans*-1,2-cyclohexanedicarboxylic (CHDA), phthalic, succinic, and maleic acids as well as oyster glycogen (GG; *M* ~7400 kDa), anthracene, triethylamine (TEA), deuterium oxide (D_2O), deuterated tetrahydrofuran (THF-d_8), Triton X-100 and phosphate-buffered saline (PBS) tablets were purchased from Sigma-Aldrich (St. Louis, MO, USA). Sodium hydrogen carbonate ($NaHCO_3$), dimethyl sulfoxide (DMSO), and toluene were purchased from Lach-Ner (Neratovice, Czech Republic), while 4-dimethylaminopyridine was purchased from Fluka (Buchs, Switzerland). Cesium chloride (CsCl) was purchased from Lachema (Brno, Czech Republic). Spectra/Por dialysis membranes with a 12-14 kDa molar mass cutoff was purchased from SpectrumLabs (Rancho Dominguez, CA, USA). All chemicals were used without further purification unless stated otherwise. 96 well plates were purchased from TPP (Trasadingen, Switzerland).

Preparation of bicyclo[2,2,2]-2,3:5,6-dibenzo-2,5-octadiene-7,8-dicarboxylic anhydride (BDODA)

Anthracene (1 g, 5.6 mmol) was mixed with toluene (30 ml) and maleic anhydride (0.5 g, 5.1 mmol) in a round bottom flask. The mixture was heated for 30 min at 75 °C with stirring (400 rpm) and the reaction proceeded for 12 h at 120 °C under reflux. After cooling to room temperature (RT) precipitated yellowish crystals were filtered off and supernatant was evaporated using vacuum-rotavapor, resulting in crude solid. Then solid phase was purified using a flash chromatography system with mobile phase consisting of ethyl acetate/pentane on stationary phase silica gel under gradient conditions with ethyl acetate content from 5 to 95 % during 1 h. Isolation resulted in 0.82 g of white powder (55 % yield). Presence of anthracene in washing solution and purity of its adduct with maleic anhydride were determined with UltiMate 3000 HPLC system (Thermo Fisher Scientific; Waltham, MA, USA), using Chromolith Performance RP 18e column and UV/VID detector.

Acylation of glycogen with selected cyclic anhydrides

Preparation of GG, modified with CHDA, BDODA, succinic, and phthalic anhydrides was done as follows. Oyster glycogen (1 g) was mixed with DMSO (10 ml), selected dicarboxylic acid anhydride (0.3 or 0.6 g), TEA (1 ml), and 4-dimethylaminopyridine (30 mg, 0.25·mmol) in a round bottom flask. The mixture was heated to 60 °C under stirring (430 rpm) for 5 h. Then the product was cooled for 10 min at RT and water (20 ml) was added. Purification was performed by dialysis against 2 L of 0.25 wt.% aqueous $NaHCO_3$ solution for 12 h, followed by triple dialysis against 2 L of pure water for 4 h each. Finally, the product was freeze-dried for 2 days, resulting in a white powder.

Solution-state ^{1}H nuclear magnetic resonance spectroscopy

Chemical structures of modified GG dissolved in D_2O were confirmed by ^{1}H NMR spectroscopy using Avance 400 MHz spectrometer (Bruker; Billerica, MA, USA).

Fourier-transformed infrared spectroscopy with attenuated total reflection (ATR-FTIR)

FTIR spectra of BDODA and modified GG samples were recorded on IFS 55 spectrometer (Bruker) equipped with Specac MKII Golden Gate single reflection ATR system on a diamond crystal, with an angle of incidence 45°, at 4 cm^{-1} resolution, 64 scans, and with an MCT detector.

Elemental analysis

Carbon, hydrogen and sodium contents in the modified GG samples were determined using the Perkin-Elmer 2400 CHN elemental analyzer and the Perkin-Elmer 3110 atomic absorption spectrometer (Beaconsfield, UK).

Dynamic light scattering (DLS) and Zeta potential measurements

In order to reveal a dependence of intensity-weighted hydrodynamic radius (R_H), scattering intensity, and zeta-potential (ζ) of dissolved modified GG and its complexes with melittin on temperature and pH, the measurements were carried out on a Zetasizer NanoZS ZEN3600 (Malvern Instruments; Malvern, UK). Concentration of modified GG was 0.72 mg/ml in citrate-phosphate buffer solution at pH 5.0, 6.0, and 7.4, while the temperature was kept at 25 ± 0.1 °C. R_H was measured at a scattering angle of $\theta = 173°$, and the data were processed with Repes algorithm, while the zeta-potential was evaluated using the model of Smoluchowski. Titration experiments were performed on the same instrument in combination with an MPT-2

autotitrator (Malvern Instruments). The concentration of titrant (HCl) was 3 M and concentrations of modified GG solutions were 0.1 mg/ml in MilliQ deionized water. During the study of GG complex formation with melittin solution as a titrant, concentrations of modified GG and melittin were 0.1 and 1.4 mg/ml, respectively. All solutions were filtered before measurement using a 0.46 μm PVDF syringe filter. Volume of GG solution was 5 ml, volume of each injection varied from 100 to 150 μl, depending on the pH of solutions, and number of injections was based on the final value of zeta-potential of solution. Each step of autotitration began from the injection of titrant, which was followed by 20 min of circulation and stirring, and finally after 10 min of sample equilibration the measurement was performed at 25 ± 0.1 °C.

Transmission electron microscopy (TEM)

Morphology of the modified GG nanoparticles was visualized by a transmission electron microscopy (TEM) using a microscope Tecnai G2 Spirit (ThermoFisher Scientific, Brno, Czech Republic). The anionized polysaccharide was stained with silver and cesium salts to increase TEM contrast. Briefly, 200 mg of CsCl and 10 mg of modified GG were dissolved in 3.8 mL of deionized H_2O in a round-bottom flask. The mixture was stirred at room temperature under 550 rpm for 12 h. The sample was dialyzed against 2 L of distilled water for 2 days to remove the excess of salts. Finally, the product was freeze-dried for 2 days, resulting in a white powder. For the TEM measurements, the stained samples were dissolved in purified water (1 mg/ml). The final samples for TEM microscopy were prepared by fast-drying method: 2 μl of the solution was dropped onto a standard carbon-coated TEM grid and left to equilibrate for 1 min. Subsequently, the excess of the solvent on the grid was removed by touching the bottom of the grid with a small piece of filter paper. This fast solution removal, which takes less than 1 s, minimizes drying artifacts as evidenced in our previous studies.[32,33] The dried samples were left to equilibrate at room temperature for 1 h and then they were observed in the TEM microscope using a bright field imaging at 120 kV.

Hemolytic assay

Human fresh whole blood in sodium citrate buffer from healthy donors was centrifuged at 423 x g for 3 min in order to remove the blood plasma. After that, red blood cells (RBCs) were washed three times with sterile phosphate buffered saline (PBS, pH = 7.4). After each washing the cells were pelleted by centrifugation at 4704 x g for 10 min and the supernatant was discarded. The final pellet was diluted with sterile PBS solution

at 1:4 (v/v) ratio. Samples of modified GG were pre-incubated with 4.5 µg/ml melittin prior to mixing with blood cells. This melittin concentration was previously established and measured to be effective concentration causing measurable hemolysis for this RBCs concentration. Suspension of RBCs at concentration ~10^8 cells/ml at final volume of 200 µl/well was then incubated in 96 well plate with diluted samples of modified GG and always constant concentration 4,5 µg/ml of melittin in PBS. Incubation was done for 1 h at 37 °C with gentle shaking. After incubation the plate was centrifuged at 2276 x g for 10 min, and 100 µl of supernatant was gently pipetted to another plate in order to measure its absorbance at 540 nm using a Synergy H1 hybrid microplate reader (BioTek Instruments, Inc., Czech Republic).

For negative controls, RBC suspension was diluted with sterile PBS. Total lysis of erythrocyte suspension was obtained by incubation of the cells with 1 % v/v of Triton X-100. For each concentration and control, the experiments were set in triplicate. In the end, three independent experiments have been performed. For calculations, 100 % of hemolysis was defined as the absorbance of positive control (Triton X-100) considered as total lysis of RBCs, while negative control with PBS was considered as 0 % of hemolysis. Hemolysis of RBCs (*H*) in % was calculated using equation

$$H = \frac{A_S - A_{NC}}{A_{PC} - A_{NC}} \cdot 100\% \quad (1)$$

where A_S, A_{NC}, A_{PC} are the absorbances of the sample, negative, and positive control, respectively. For calculating the inhibitory effect of GG encapsulators in the samples with melittin, total values of H were recalculated in regard to the value of H caused by melittin alone, which was considered as 0% of inhibition.

Statistical analysis

Data are presented as the mean ± standard error of the mean (S.E.M.). Statistical significance of differences in the inhibition of hemolysis was calculated by a nonparametric one-way ANOVA with Dunnett's post-hoc test using GraphPad Prism version 5.03 (GraphPad software, La Jolla, CA, USA), $p < 0.05$ was considered as statistically significant. Comparison of effects caused by individual samples of modified GG was tested by one-way ANOVA and Bonferroni multiple comparison post-hoc test at significance level $p < 0.05$.

IC_{50} values were calculated using GraphPad Prism version 5.03 (GraphPad software, La Jolla, CA, USA) by fitting the Hill equation to the experimental data. The Hill equation[34] describes the effect *E* obtained at a given concentration of a drug, *C*, as

$$E = E_0 + \frac{E_\infty - E_0}{1 + (EC_{50}/C)^H} \quad (2)$$

where EC_{50} is the concentration at which 50% of the maximum effect is achieved, H is the Hill exponent, E_∞ is the maximum effect and E_0 is the effect in the absence of the drug. The EC_{50} is sometimes called ED_{50} (effective dose), or IC_{50} (inhibitory concentration). The Hill exponent sometimes called the slope factor or the Hill coefficient.

RESULTS AND DISCUSSION

Synthesis and characterization of substituted glycogens

In order to produce a biodegradable well-defined encapsulator of polycationic cargos, a series of modified anionic glycogens were synthesized by acylation of oyster glycogen (GG) with selected dicarboxylic acid anhydrides, possessing different hydrophobicity (BDODA, CHDA, phthalic and succinic anhydrides). Two different degrees of substitution were prepared from each anhydride to assess the effect of charge density. The biodegradation therefore occurs on the glycoside bonds (polysaccharide to monosaccharide) and ester bonds (hydrolysis to glucose unit and diacid). The detailed description of synthesis is given in the experimental section. Names and yields of obtained modified GG samples are shown in Table 1, and their structures are presented in Figure 1.

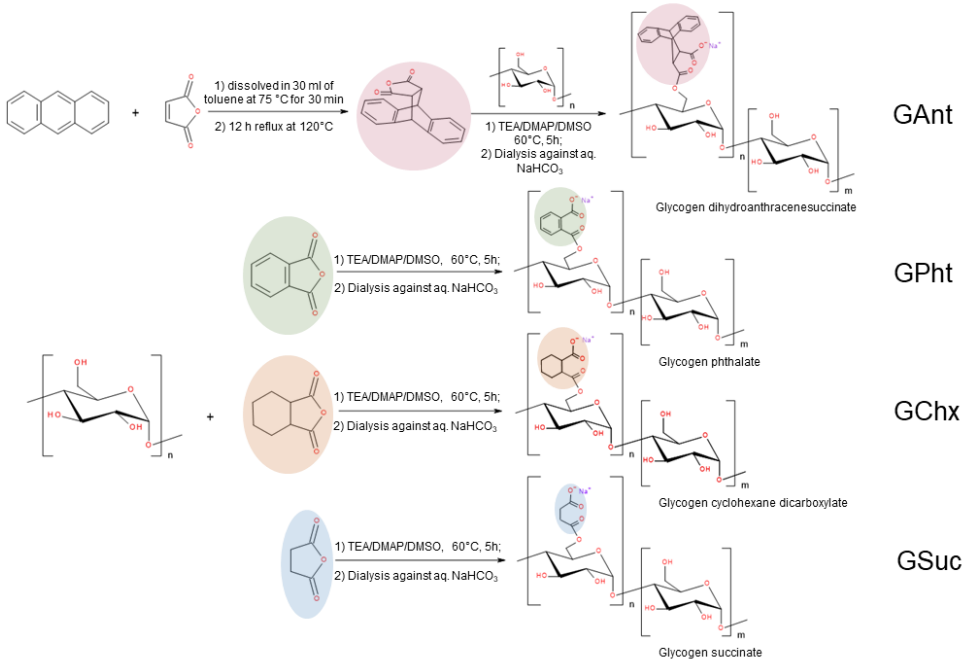

Figure 1. Scheme of glycogen modification with anhydrides of dicarboxylic acids. Note that the functional groups may be attached to various positions on the glucose unit.

The degree of substitution (D_S) of GG hydroxyls with dicarboxylic acid residues (Table 2) was determined from the content of sodium cations that neutralized the carboxyl groups during the purification process, using the equation

$$D_s = \frac{n_{\text{anh.}}}{n_{\text{gluc.}}} = \frac{m_{\text{Na}}/M_{\text{Na}}}{m_{GG}/M_{\text{gluc.}}} = \frac{w_{\text{Na}}/M_{\text{Na}}}{[100 - w_{\text{Na}} \cdot (1 + M_{\text{anh.}}/M_{\text{Na}})]/M_{\text{gluc.}}} \quad (3)$$

where *n*, *m*, *w*, and *M* are the amount of substance, mass, mass percent composition, and molar mass, respectively. The subscript "anh." stands for "anhydride", and "gluc." stands for "glucose unit". For this purpose, the contents of carbon, hydrogen and sodium were determined by elemental analysis, that was in good agreement with their theoretical content, calculated from the composition of the reaction mixture (for details, see Supporting information, Table S1). The sodium content and the degree of substitution diminished with increasing hydrophobicity of the anhydrides, as evidenced by the data in Table 1. From the degrees of substitution, we calculated molar mass of the modified glycogens according to the equation

$$M = M_0 \cdot (1 + M_{anh.} \cdot D_s/M_{\text{gluc.}}) \quad (4)$$

where D_S is the degree of substitution and M_0 = 7400 kDa is the molar mass of pure glycogen. As expected, the highest degree of substitution was achieved for the sterically most accessible succinate, a lower one was achieved for the more hydrophobic and sterically hindered phthalate and cyclohexane dicarboxylate, and the lowest one for the sterically most hindered and most hydrophobic dihydroanthracenesuccinate. The chemical structure of modified glycogens was further confirmed by ATR-FTIR and ^{1}H NMR spectra (see Supporting Information, Figures S1 and S2).

Table 1. Properties of the synthesized samples of modified glycogens.

Full name	Abbre-viation[a]	Initial Anhydride/GG mass ratio	Yield, %	Resultant Degree of substitution[b]	Molar mass[c], kDa
Glycogen succinate	GSuc380	0.3/1	81	0.380	9140
	GSuc685	0.6/1	95	0.685	10530
Glycogen phthalate	GPht165	0.3/1	71	0.165	8520

	GPht285	0.6/1	70	0.285	9320
Glycogen cyclohexane dicarboxylate	GChx110	0.3/1	53	0.110	8180
	GChx265	0.6/1	45	0.265	9270
Glycogen dihydro-anthracenesuccinate	GAnt014	0.3/1	46	0.014	7580
	GAnt038	0.6/1	45	0.038	7890

[a] The sample abbreviations are composed of GG for glycogen, three letters Xxx for the type of functional group (Suc, Pht, Chx, Ant) and three digits YYY for the degree of substitution (digits following the leading zero); [b] estimated from the content of Na as described in the text; [c] calculated from the corresponding degrees of substitution and known molar mass of unmodified glycogen.

The effect of pH and degree of substitution on the melittin-glycogen interaction

Because the functional groups on the glycogens are weak acids, their ionization state depends on the pH, which in turn crucially affects the ability of these conjugates to encapsulate melittin. The effective pK_a of polyacids is usually higher and consequently their charge is typically lower than that of their parent monomers at the same pH value.[35-40] In polyelectrolytes with both positive or negative charges,[41,42] upon interaction with oppositely charged multivalent ions[43] or with other polyelectrolytes[41] the ionization states depend not only on the pK_a values of individual acid and base groups but also on their distribution on the chain and on the conformation of the macromolecule.[42] In such a complex case, the resultant ionization can be difficult to estimate from simple theories, such as the Henderson-Hasselbalch equation, however, it can be analyzed using a molecular simulation.[44,45]

To investigate the effect of pH and degree of substitution on the ability of modified glycogens to encapsulate melittin, we constructed a simplified molecular model. Within this model, the functionalized glycogen is represented as a hyperbranched polymer, with G = 5 generations and N = 6 beads between the branching points, as illustrated by the schematic and simulation snapshot in Figure 3. In total, the model dendrimer consisted of 373 monomeric units, represented as spherical beads. It was necessary to make the model much smaller than its experimental counterpart in order to make the simulation computationally feasible. Only a certain fraction of the glucose units was functionalized and treated as weak acids with variable protonation states depending on their pK_a, pH and on the local environment. The weak acid groups were distributed homogeneously within the whole dendrimer structure, whereas and the remaining (non-functionalized) monomeric units were neutral. Melittin was modelled as a chain of beads, each of which represented one amino

acid residue, as sketched in Figure 3. Two extra beads accounted for the acid and base groups at the C- and N-terminus, respectively. Steric repulsion was included in the model, whereas hydrophobic interactions were not included. For simplicity, all beads had the same interaction parameters, except for their acid-base properties, defined by the pK_a values listed in Table 2.

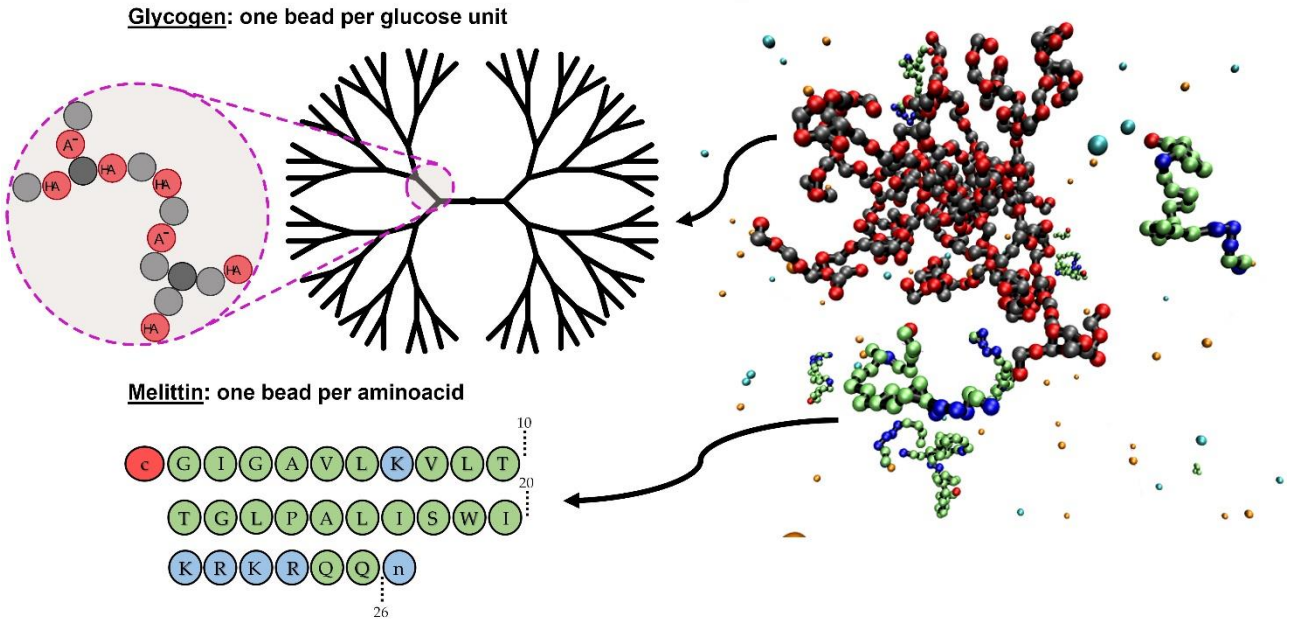

Figure 3. Left: Scheme of the models used for glycogen (top) and melittin (bottom). Right: snapshot from a simulation at pH = 7.5. Color code: acidic bead (red), basic bead (blue), neutral bead of the glycogen (grey), neutral bead of melittin (green), Na^+ cation (cyan) and Cl^- anion (orange).

Table 2. List of the pK_a values for the acidic/basic beads for melittin and glycogen, namely: glucose group functionalized by a weak-acid moiety (HA), lysine (LYS), arginine (ARG) and the carboxylic (COOH) and amino (NH_2) terminus. The pK_a values for the aminoacid residues are taken from Ref.[46]

HA	-COOH	-NH_2	-LYS-	-ARG-
4.25	3.60	8.00	10.4	13.5

It could be easily guessed that acid-functionalized glycogens should attract multivalent cationic peptides, such as melittin, however, it is not so obvious whether this attraction is strong enough to effectively encapsulate melittin in the dendrimer structure. The strength is of this attraction depends on the total charge on each of the macromolecules. Therefore, functionalized glycogen can act as an efficient encapsulator only if it is sufficiently charged. The amount of charge on the modified glycogens depends on two key parameters: the degree of substitution by acidic groups, and the degree of ionization of these groups. The former is determined at the time of synthesis, whereas the latter depends on the pH and on pK_a of the functional groups. Thus, the key question is what amount of charge is sufficient, and under what conditions it can be achieved.

To answer this question by molecular simulations, we first examine the total charge on melittin and on the functionalized dendrimer with $D_s = 0.5$ as a function of pH, shown in Figure 4. For the dendrimer, we selected $pK_a = 4.25$ as a typical value to represent the carboxylate functional groups used in our experiments. Figure 4 shows that the charge on both dendrimer and melittin is much lower than the ideal result obtained using the Henderson-Hasselbalch equation. This difference is caused by electrostatic repulsion between the like-charged groups within each of these molecules. In the case of the dendrimer, it results in the effective $pK_a \sim 6$, which is close to pH ~ 5-7, relevant for the encapsulation experiments. In the case of melittin, the difference is significant only at pH > 6, corresponding to the ionization of the N-terminus, lysine and arginine groups, which are close to each other in the melittin sequence (see Fig.1). On the contrary, the C- terminus is far from the other charged groups, therefore, its ionization is not affected by their presence, and melittin follows the ideal curve at a low pH<5.

Furthermore, Figure 4 shows that ionization of the dendrimer is only negligibly affected by the presence of melittin and vice versa. This observation differs from previous observations in the simulation literature that interactions with multivalent ions significantly increase the ionization states of polyelectrolytes, which is accompanied by a collapse of their conformation.[36,37] This difference is presumably caused by rather low charge density in the hyperbranched polymer with degree of functionalization $D_s = 0.5$ and by steric repulsion due to neutral groups on melittin which prevent the collapse. However, close to the physiological pH, the dendrimer is almost fully charged, and the melittin charge is around $+4e$. By analogy with our previous publication[36] this charge should suffice for rather strong encapsulation.

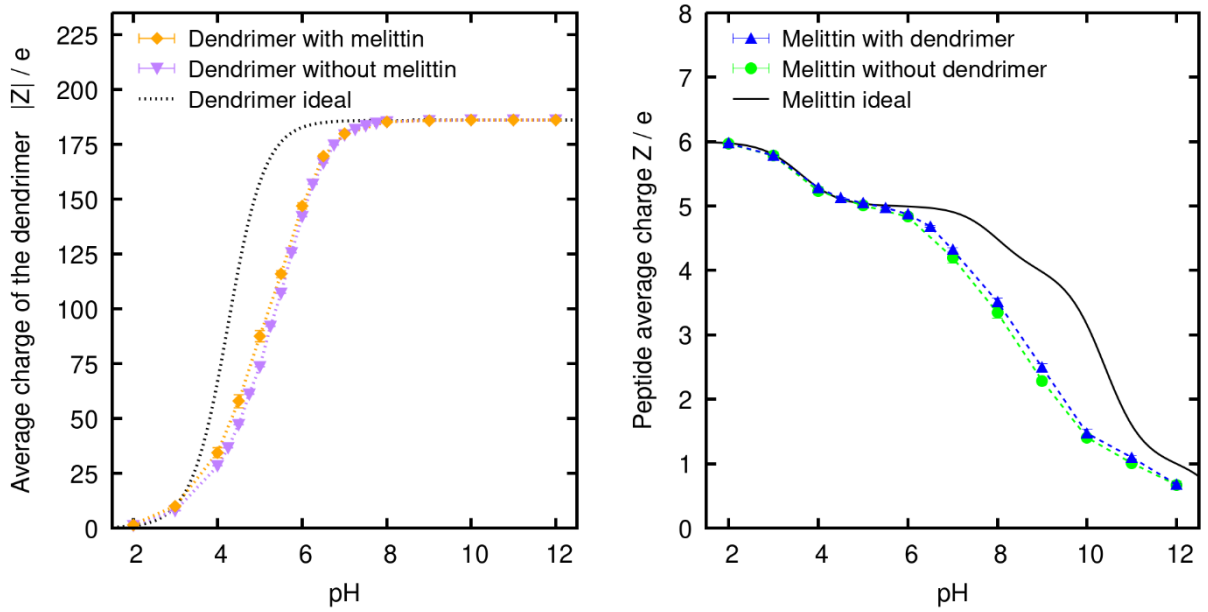

Figure 4. Average charge *Z* of the dendrimer (left panel) and melittin (right panel) as a function of pH. Different data sets represent: (i) Melittin in absence of the dendrimer (circles), (ii) the dendrimer in absence of melittin (downward triangles) and (iii) the dendrimer (diamonds) and melittin (upwards triangles) together in solution. Black lines show the ideal titration curve for the dendrimer (continuous line) and melittin (dotted line) given by Eqs. S7 and S8.

To quantify the ability of the dendrimer to encapsulate melittin, we can use concentration profiles of all ionic species as a function of distance from the dendrimer core at selected pH values, shown Figure 5. In all cases, melittin concentration close to the core is several orders of magnitude higher than in the bulk (far from the core). This difference is much greater than in the concentration profiles of monovalent cations, indicating efficient encapsulation of melittin by the dendrimer. In addition, the difference in melittin concentrations inside and outside the dendrimer is greater at pH = 7.5 than at pH = 4 and 10, indicating that the encapsulation is particularly strong close to the physiological pH.

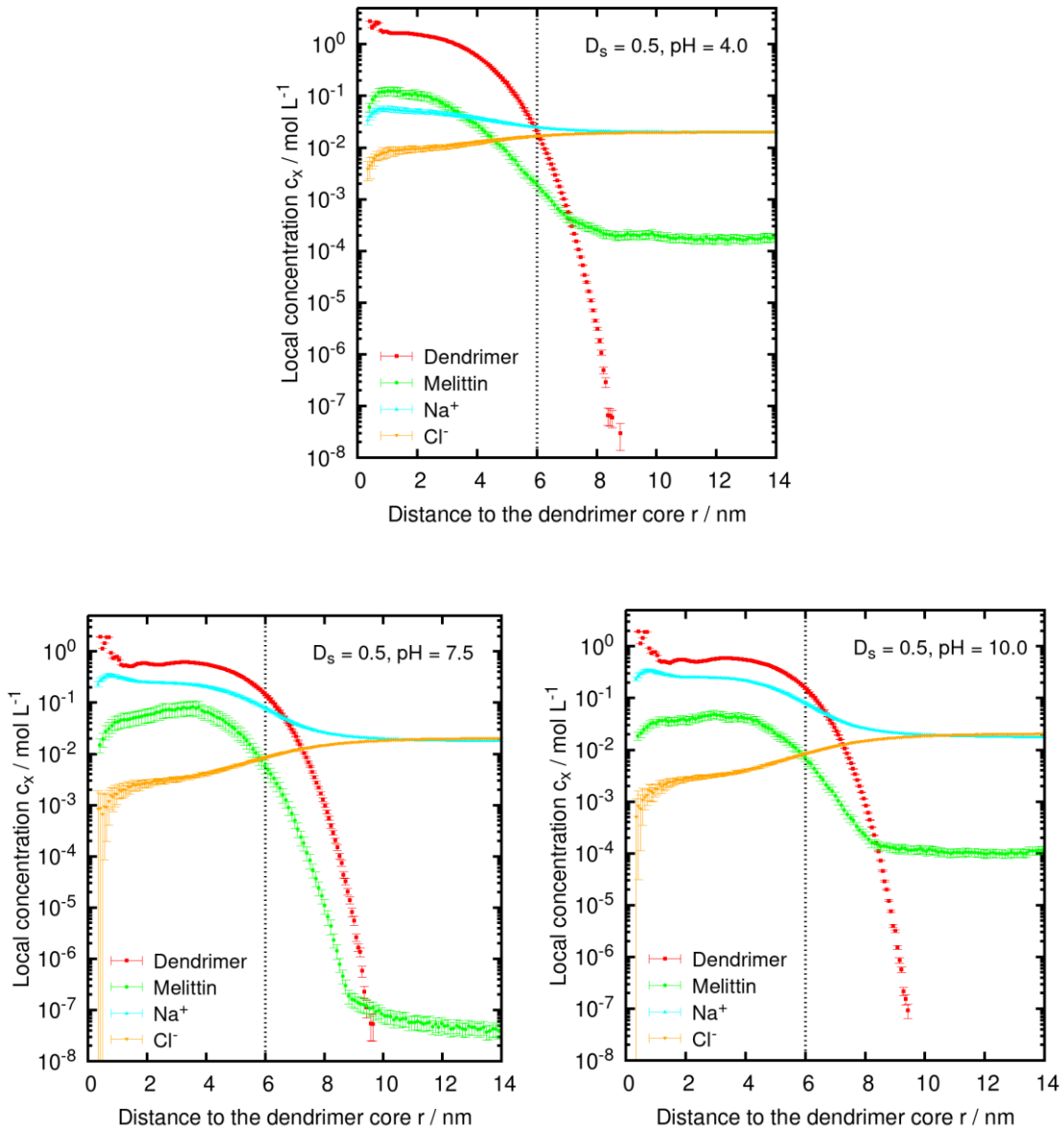

Figure 5. Concentration profiles of various ionic species, plotted as a function of distance from the core of the dendrimer r. The results correspond to degree of substitution of glycogen $D_s = 0.5$ and the following pH values: 4.0, 7.5 and 10.0. The vertical dashed line at r = 6nm denotes the boundary between interior and exterior of the dendrimer, used for the calculation of adsorption coefficient.

The efficiency of encapsulation can be further quantified in terms of partition coefficient $K = c_{ads} / c_{free}$, where c_{ads} and c_{free} refer to the average concentration of melittin inside and outside the hyperbranched polymer (see Supporting Information for details of how the average concentrations were determined). Figure 6 shows the computed partition coefficients as a function of pH, demonstrating that encapsulation of melittin by the model dendrimer is very efficient in a broad range 4.5 < pH < 9.0 that extends over the whole biologically relevant

range. This range can be considered as the optimal pH conditions for efficient encapsulation of melittin by acid-functionalized glycogens.

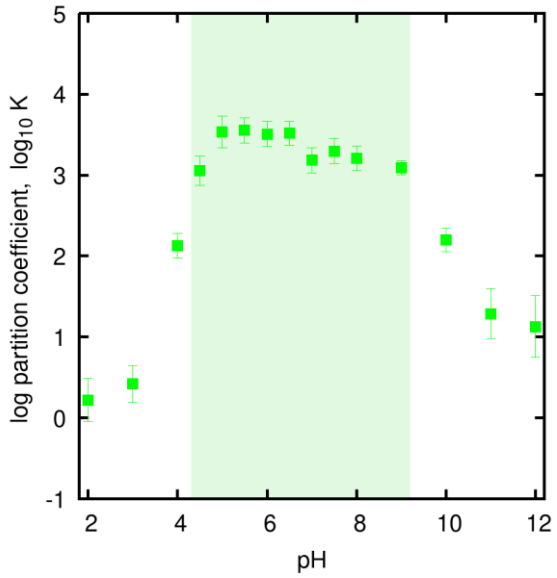

Figure 6. Partition coefficient $log_{10}\ K$ of melittin encapsulated by the model dendrimer at various pH values. The shaded area indicates the estimated optimum pH range for encapsulation.

If the degree of functionalization of the dendrimer is decreased from $D_s = 0.5$ to $D_s = 0.05$, its ionization as a function of pH increases and approaches the ideal curve, suggesting that the optimum pH range for encapsulation of melittin might be even broader. However, Figure 7 reveals that, although the dendrimer with $D_s = 0.05$ is fully ionized at pH = 7.5, the concentration profile of melittin is much flatter than in Figure 5. In addition, our simulation results in Fig.S5 demonstrate that glycogen functionalized to an intermediate degree, $D_s = 0.25$, is still able to encapsulate melittin close to the neutral pH, whereas its encapsulation capability diminishes if the pH becomes more acidic or more basic. These results demonstrate that acid-functionalized dendrimers can efficiently encapsulate melittin only beyond a certain a minimal degree of functionalization, whereas dendrimers with a low degree of functionalization cannot efficiently encapsulate it even at the optimum pH.

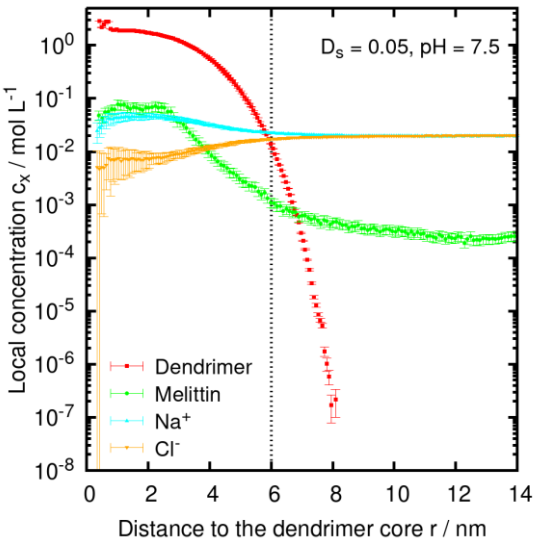

Figure 7. Concentration profiles of various ionic species, plotted as a function of distance from the core of the dendrimer r. The results correspond to degree of substitution of the dendrimer D_s = 0.05 and following pH = 7.5.

We titrated selected glycogen samples by melittin to verify whether the simulation predictions, based on a simplified model, are applicable to describe the interactions of melittin with our acid-functionalized glycogens. We fixed the pH during the titrations at pH = {5.0, 6.0, 7.4}, in order to cover the whole pH range relevant for the intended biological application, starting from 5 (late endosome after internalization into cells) up to 7.4 (blood plasma). During these titrations, we simultaneously followed the hydrodynamic radius and zeta potential as a function of the mass ratio melittin / modified glycogen. In Figure 8, we show the results of these titrations for GPht285 at three pH values. Analogous results for GSuc685 and GChx265 are provides in the Supporting Information. Because these titrations were demanding, we selected samples with the higher degree of substitution for each type of the functional group, assuming that they are the most promising candidates. Furthermore, we excluded the anthracene-functionalized samples because preliminary results of the biological experiments indicated that these samples were not able to inhibit melittin.

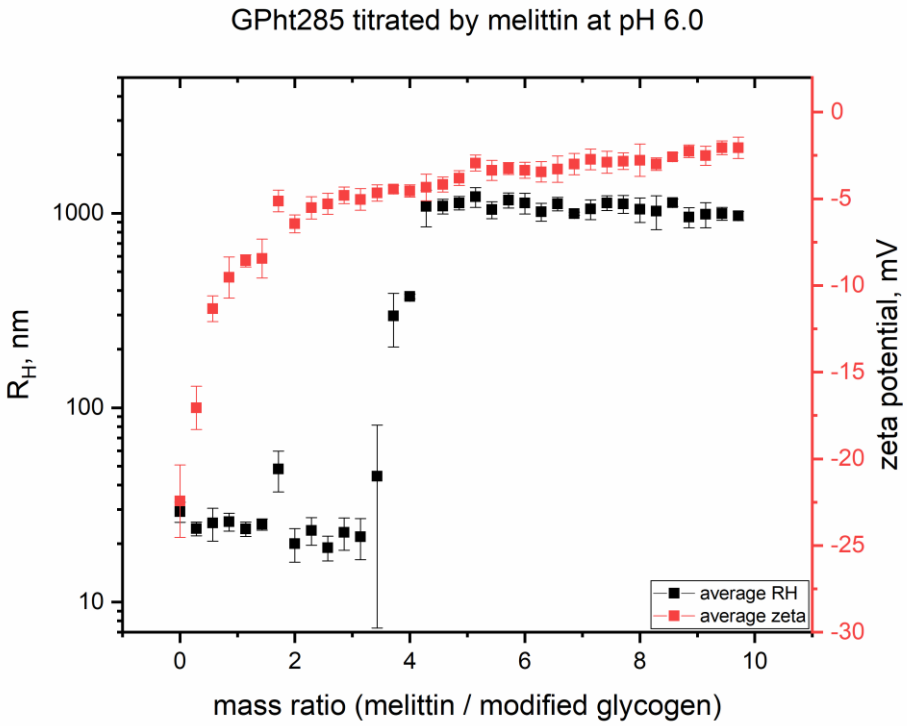

Figure 8. Hydrodynamic radii and zeta potentials of acid-functionalized glycogen GPht285 (c_{glyc} = 0.1 mg/mL) titrated by melittin (c_{mel} = 1.4 mg/mL) at various pH values. Analogous results for other samples are provided in the Supporting Information, Fig.S6 and S7.

According to Figure 8, as melittin is being added to the acid-functionalized glycogen GPht285, the zeta potential increases sharply at the early stage of the titration, and then continues to increase less steeply throughout the rest of the experiment. This increase indicates that the acid-functionalized glycogen acquires extra positive charge by encapsulating melittin. In contrast with the zeta potential, the hydrodynamic radius is initially unaffected by the addition of melittin. Its values on the order of 20-50 nm clearly demonstrate that the functionalized glycogens are dissolved as individual molecules (unimers). In a later stage, we observed a sudden increase in the measured hydrodynamic radius that attains values on the order of 1000 nm, indicating the formation of huge clusters containing many glycogen molecules. Similar behavior was observed for GChx265, whereas GSuc685 exhibited a less abrupt increase of Rh (see Supporting Information, Fig.S6). We can deduce from the comparison of the trends in Rh(pH) and zeta(pH) that, at low mass ratio, the modified glycogen efficiently encapsulated melittin inside the hyperbranched structure, while it simultaneously retained sufficient negative charge that prevented aggregation. At a certain threshold, the encapsulation capacity of the modified glycogen becomes saturated, a further addition of melittin presumably caused adsorption on the

surface of the glycogen particles by a combination of electrostatic interactions and hydrophobic interactions with the hydrophobic part of the melittin sequence. The hydrophobic melittin adsorbed on the glycogen surface then act as a crosslinker, bridging many glycogen particles into much bigger aggregates. Control experiments confirmed that melittin adsorbs only on the modified glycogens because such aggregation did not occur if unmodified glycogens were titrated by melittin (cf. Fig.S7). Irrespective of the details of the mechanism of melittin encapsulation and subsequent aggregation, the most important observation from the DLS titrations is that the acid-functionalized glycogen nanoparticles can efficiently encapsulate melittin in the amount that several times exceeds the mass of the modified glycogen. The threshold mass ratios of melittin / modified glycogen, at which the particles started to aggregate, are listed in Table 3. These threshold values can be used as indicators of the upper limit, up to which various acid-functionalized glycogen samples are able to efficiently encapsulate melittin. Based on these limits, GPht seems to be slightly more efficient encapsulator than GChx and GSuc. However, the values obtained for all these samples are within the same order of magnitude, suggesting that the type of substituent (Pht, Suc or Chx) has little effect on the encapsulation ability. Therefore, all these samples can be considered as promising candidates for the intended application, and their true ability to efficiently inhibit the hemolytic activity of melittin should be verified directly.

Table 3. The mass ratio of melittin/glycogen at which the big aggregates start to form.

Sample name	pH		
	5.0	**6.0**	**7.4**
GChx265	1.54 ± 0.14	0.29 ± 0.29	1.89 ± 0.21
GPht285	3.29 ± 0.14	3.86 ± 0.43	4.08 ± 0.21
GSuc685	1.29 ± 0.42	2.24 ± 0.56	2.72 ± 0.71

Inhibition of melittin's hemolytic activity by the substituted glycogens

We used a hemolytic assay to quantify the ability of acid-functionalized glycogens to bind and inhibit the hemolytic toxin melittin. Figure 9 shows that the glycogens with a higher degree of substitution (GSuc685, GPht285 and GChx265) inhibit the hemolytic activity of melittin at a statistically significant level. The glycogen GPh165 with a lower degree of substitution also significantly inhibited the activity of melittin. Another low-substituted sample, GChx110, significantly inhibited the activity of melittin only at higher

concentrations of glycogen. In contrast, GSuc380 did not inhibit melittin, despite a rather high degree of substitution, however, the trend in Figure 9 suggests that GSuc380 might inhibit melittin at higher concentrations. Finally, the anthracene-based samples GAnt014 and GAnt038 did not have any measurable effect on the hemolytic activity of melittin. Thus, the hemolytic assay has demonstrated that the type of substituent has a significant effect on the ability of acid-functionalized glycogens to inhibit melittin, contrasting with the previous observation that the type of substituent has little effect on the encapsulation ability (*cf.* Fig. 8).

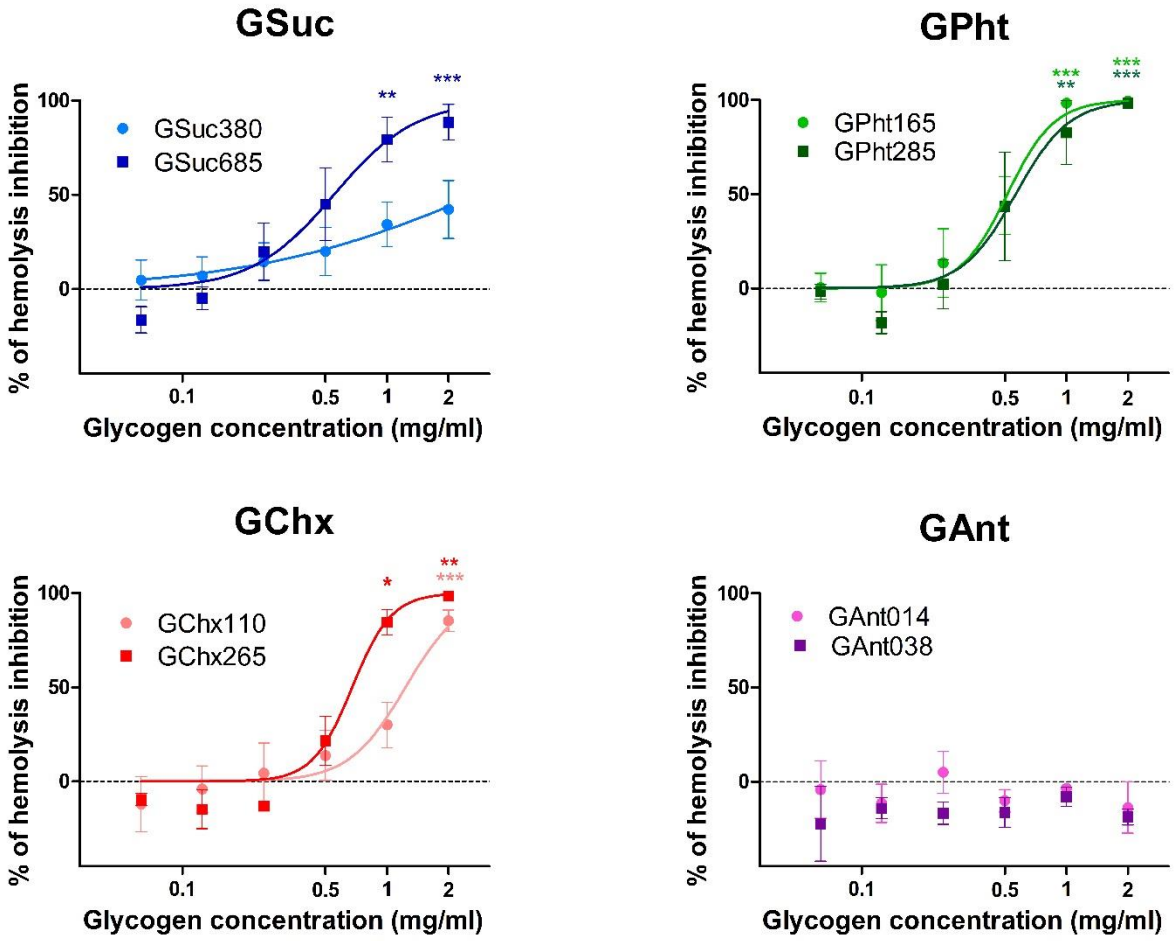

Figure 9. Inhibition of hemolytic activity of melittin by acid-functionalized glycogens. Lines show dose response curves obtained as fits to the data points. Asterisks indicate statistically significant differences of the measured values compared to the control value on the following levels of significance: * $p \leq 0.05$; ** $p \leq 0.01$; *** $p \leq 0.001$.

In Figure 10 we compare the concentrations of acid-functionalized glycogens causing 50% inhibition of melittin's hemolytic activity, IC_{50}, obtained by fitting dose-response curves to the data from Figure 9. For some samples, IC_{50}, could not be calculated reliably because their IC_{50} is higher than the highest tested concentration (GSuc380) or their hemolytic activity was not detected (GAnt). Among the remaining samples, we can observe that IC_{50} of GSuc685, GPht285 and GChx265 is the same within the estimated uncertainty, in agreement with comparable threshold values of mass ratios melittin / modified glycogen, listed in Table 3. A plot of the IC50 value as a function of the degree of functionalization (Fig.S8) confirms that a low IC50 can be achieved beyond a certain threshold degree of functionalization. Interestingly, the low-substituted GPht165 has the same value of IC_{50} within the estimated uncertainty, whereas GChx110 has a slightly higher IC_{50}. Thus, we conclude that five of our samples (GSuc685, GPht285, GPht165, GChx265, GChx110) inhibit melittin's hemolytic activity *in vitro* and should be considered as candidates for further application-oriented investigations.

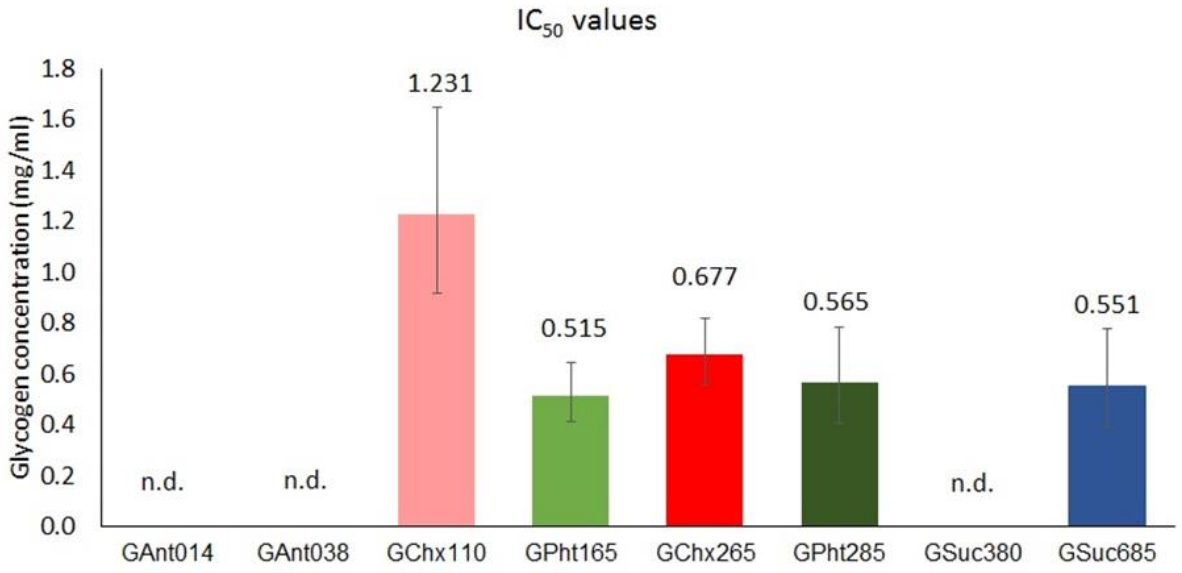

Figure 10. Calculated IC_{50} values for each acid-functionalized glycogen sample. Error bars indicate 95% confidence interval. Values that could not be reliably defined are marked as "n.d.".

CONCLUSIONS

We proposed novel biocompatible anionic encapsulators, based on acid-functionalized glycogens. The key aspect of their encapsulation ability is multivalent electrostatic interaction with cationic cargos. We

synthesized a set of samples with various functional groups and various degrees of substitution, characterized their physico-chemical properties using a combination of molecular simulations and experiments, and finally demonstrated *in vitro* that the prepared samples inhibit hemolytic activity of a model cationic toxin melittin, which is the key component of honeybee venom. Five of these samples effectively inhibited its activity at concentrations of the functionalized glycogens as low as 0.5 mg/ml, proving that they are promising candidates for the intended application as honeybee venom antidote.

In the synthesis, we have achieved the highest degrees of substitution in glycogens modified by succinate functional groups (30-70%), slightly lower with phthalate and cyclohexyl (10-30%) and very low with anthracene-based groups (below 1%). Subsequently, our molecular simulations have shown that electrostatic interactions between acid-functionalized glycogens and melittin should result in a strong encapsulation in a broad pH range between 4 and 9, safely extending over and beyond the pH range relevant for the intended application, from 5 to 7.4. Furthermore, the simulations have shown that glycogens with a low degree of substitution cannot efficiently encapsulate melittin even at the optimum pH. In the sequel, we titrated the high-substituted glycogen by melittin to confirm their encapsulation ability. By following the hydrodynamic radius and zeta potential as a function of mass ratio melittin / modified glycogen, we observed that these samples efficiently encapsulated melittin up to a certain threshold, beyond which they start aggregating. The value of this threshold only weakly depended on the type of substituent, showing that all high-substituted samples could encapsulate an amount of melittin that exceeds their own mass by 2-4 times. Finally, we evaluated the ability of all acid-functionalized glycogens to inhibit hemolytic activity of melittin *in vitro*. For most of our samples, we determined IC_{50} about 0.5 mg/ml. However, we observed significant differences when comparing various substituents and degrees of substitution. Glycogens functionalized by phthalate attained this value of IC_{50} at 26% and 11% functionalization, cyclohexyl-functionalized glycogens attained it at 26%, whereas succinyl-functionalized glycogens attained it only at 68% functionalization. Cyclohexyl-functionalized at 11% had a higher IC_{50}, whereas succinyl-functionalized ones at 38% had IC_{50} beyond the studied range of concentrations. Finally, anthracene-functionalized glycogens did not exhibit any inhibition activity at all, which could be attributed to their low degree of substitution (below 1%).

Ultimately, we have obtained biodegradable, easy to prepare and relatively inexpensive functional carriers based on acid-functionalized glycogens. Five of them (GSuc685, GPht285, GPht165, GChx265, GChx110) efficiently encapsulate melittin and inhibit its hemolytic activity at rather low concentrations. These samples

should be used in further studies, addressing their potential application as antidotes for honeybee and other animal venoms. In addition, our computer simulations and physicochemical characterization demonstrated that encapsulation based on multivalent electrostatic interactions extends the applicability of acid-functionalized glycogens beyond the specific case of melittin. They should be able to efficiently encapsulate also other cationic cargos, such as antibiotics (*e.g.*, polymyxin B or kanamycin), cationic peptides and proteins or other moderately-sized multivalent cationic objects.

Supporting information: Details on the computational model; additional details on characterization of the prepared glycogen conjugates by ATR-FTIR, ^{1}H NMR, DLS and Zeta potential measurements.

ACKNOWLEDGEMENTS

H.Z., Z.C., J.P., P.B., M.S., P.K. acknowledge the financial support from the Czech Science Foundation, grant 19-10429S; M.F. and M.H. acknowledge the grant 21-04166S. RS acknowledges financial support by the Doctoral College Advanced Functional Materials - Hierarchical Design of Hybrid Systems DOC 85 funded by the Austrian Science Fund (FWF). Computational resources were provided by the project "e-Infrastruktura CZ" (e-INFRA CZ LM2018140) supported by the Ministry of Education, Youth and Sports of the Czech Republic.

REFERENCES

1. G. Gajski, V. Garaj-Vrhovac, Melittin: A lytic peptide with anticancer properties. *Env. Toxicol. Pharm.* **2013**, *36*, 697-705.

2. G. Lee, H. Bae, Anti-inflammatory applications of melittin, a major component of bee venom: Detailed mechanism of action and adverse effects. *Molecules* **2016**, *21*, 616, 1-10.

3. S. Hossen, S. Gan, I. Khalil, Melittin, a potential natural toxin of crude bee venom: Probable future arsenal in the treatment of diabetes mellitus. *J. Chem.* **2017**, *2017*, 1-7.

4. I. Al-Ani, S. Zimmermann, J. Reichling, M. Wink, Pharmacological synergism of bee venom and melittin with antibiotics and plant secondary metabolites against multi-drug resistant microbial pathogens. *Phytomedicine* **2015**, *22*, 245-255.

5. H. Memariani, M. Memariani, H. Moravvej, M. Shahidi-Dadras, Melittin: A venom-derived peptide with promising anti-viral properties. *Eur. J. Clin. Microbiol. Infect. Dis.* **2019**, *39*, 5-17.

6. N. Soman, G. Lanza, J. Heuser, P. Schlesinger, S. Wickline, Synthesis and characterization of stable fluorocarbon nanostructures as drug delivery vehicles for cytolytic peptides. *Nano Lett.* **2008**, *8*, 1131-1136.

7. M. Tissera, E. Disalvo, M. Martini, A. Cutró, Filling gaps in the knowledge of melittin on lipid membranes. *Col. Surf. A* **2018**, *561*, 136-146.

8. S. Blondelle, L. Simpkins, E. Pérez-Payá, R. Houghten, Influence of tryptophan residues on melittin's hemolytic activity. *Biochim. Biophys. Acta* **1993**, *1202*, 331-336.

9. A. Oddo, P. Hansen, Hemolytic activity of antimicrobial peptides. *Methods Mol. Biol.* **2017**, *1548*, 427-435.

10. D. Raymond, B. Nilsson, Multicomponent peptide assemblies. *Chem. Soc. Rev.* **2018**, *47*, 3659-3720.

11. A. Światły-Błaszkiewicz, L. Mrówczyńska, E. Matuszewska, J. Lubawy, A. Urbański, Z. Kokot, G. Rosiński, J. Matysiak, The effect of bee venom peptides melittin, tertiapin, and apamin on the human erythrocytes ghosts: A preliminary study. *Metabolites* **2020**, *10*, 191, 1-13.

12. H. Raghuraman, A. Chattopadhyay, Melittin: A membrane-active peptide with diverse functions. *Biosci. Rep.* **2007**, *27*, 189-223.

13. M.T. Tosteson, S. J. Holmes, M. Razin, D.C. Tosteson, Melittin lysis of red cells. *J. Membr. Biol.* **1985**, *87*, 35-44.

14. N. Doshi, S. Mitragotri, Designer biomaterials for nanomedicine. *Adv. Funct. Mater.* **2009**, *19*, 3843-3854.

15. J. Feng, R. Zhu, F. Jiang, D. Fu, Melittin-encapsulating peptide hydrogels for enhanced delivery of impermeable anticancer peptides. *Biomat. Sci.* **2020**, *8*, 4559 –4569.

16. H. Jia, Y. Zhu, K. Xu, F. Wu, Turning toxicants into safe therapeutic drugs: Cytolytic peptide-photosensitizer assemblies for optimized in vivo delivery of melittin. *Adv. Healthcare Mater.* **2018**, *7*, 1-11.

17. N. Doshi, S. Mitragotri, Designer biomaterials for nanomedicine. *Adv. Funct. Mater.* **2009**, *19*, 3843-3854.

18. M. S. Alkanawati, R. da Costa Marques, V. Mailänder, K. Landfester, H. Thérien-Aubin, Polysaccharide-Based pH-Responsive Nanocapsules Prepared with Bio-Orthogonal Chemistry and Their Use as Responsive Delivery Systems. *Biomacromolecules* **2020**, *21*, 2764–2771.

19. A. Gálisová, M. Jirátová, M. Rabyk, E. Sticová, M. Hájek, M. Hrubý, D. Jirák, Glycogen as an advantageous polymer carrier in cancer theranostics: Straightforward in vivo evidence. *Sci. Rep.* **2020**, *10*, 10411, 1-11.

20. S. Sreekumar, F. Goycoolea, M. Moerschbacher, G. Rivera-Rodriguez, Parameters influencing the size of chitosan-TPP nano- and microparticles. *Sci. Rep.* **2018**, *8*, 4695, 1-12.

21. C. Goh, P. Heng, L. Chan, Alginates as a useful natural polymer for microencapsulation and therapeutic applications. *Carbohydr. Polym.* **2012**, *88*, 1-12.

22. M. Collins, C. Birkinshaw, Hyaluronic acid based scaffolds for tissue engineering – A review. Carbohydr. *Polym.* **2013**, *92*, 1262-1279.

23. S. Huang, G. Huang, Preparation and drug delivery of dextran-drug complex. Drug Deliv. **2019**, *26*, 252-261.

24. C. Paleos, Z. Sideratou, D. Tsiourvas, Drug delivery systems based on hydroxyethyl starch. *Bioconjug. Chem.* **2017**, *28*, 1611-1624.

25. M. Bertoldo, G. Zampano, L. Suffner, E. Liberati, F. Ciardelli, Oxidation of glycogen "molecular nanoparticles" by periodate. *Polym. Chem.* **2013**, *4*, 653-661.

26. Q. Besford, F. Cavalieri, F. Caruso, Glycogen as a building block for advanced biological materials. *Adv. Mater.* **2019**, *32*, 1-23.

27. S. Filippov, O. Sedlacek, A. Bogomolova, M. Vetrik, D. Jirak, J. Kovar, J. Kucka, S. Bals, S. Turner, P. Stepanek, M. Hruby, Glycogen as a biodegradable construction nanomaterial for in vivo use. *Macromol. Biosci.* **2012**, *12*, 1731-1738.

28. P. Melamed, F. Melamed, Chronic metabolic acidosis destroys pancreas. *J. Pancreas* **2014**, *15*, 552-560.

29. R. Lunkad, A. Murmiliuk, P. Hebbeker, M. Boublík, Z. Tošner, M. Štěpánek, P. Košovan, Quantitative prediction of charge regulation in oligopeptides. *Mol. Sys. Des. Eng.* **2021**, *6*, 122-131.

30. R. Lunkad, A. Murmiliuk, Z. Tošner, M. Štěpánek, P. Košovan, Role of pKA in Charge Regulation and Conformation of Various Peptide Sequences. *Polymers* **2021**, *13*, 214, 1-21.

31. P.M. Blanco, S. Madurga, J.L. Garcés, F. Mas, R.S. Dias, Influence of macromolecular crowding on the charge regulation of intrinsically disordered proteins. *Soft Matter* **2021**, *17*, 655-669.

32. O. Paiuk, N. Mitina, M. Slouf, E. Pavlova, N. Finiuk, N. Kinash, A. Karkhut, N. Manko, T. Gromovoy, O. Hevus, Y. Shermolovich, R. Stoika, A. Zaichenko, Fluorine-containing block/branched polyamphiphiles forming bioinspired complexes with biopolymers. *Colloids Surf. B* **2019**, *174*, 393–400.

33. Kolouchova K., Groborz O., Cernochova Z., Skarkova A., Brabek J., Rosel D., Svec P., Starcuk Z., Slouf M., Hruby M., Thermo- and ROS-responsive self-assembled polymer nanoparticle tracers for 19F MRI theranostics. *Biomacromol.* **2021**, *22*, 2325-2337.

34. A.V. Hill, The possible effects of the aggregation of the molecules of haemoglobin on its dissociation curves. *J. Physiol.* **1910**, *40*, 4-7.

35. L. Nová, F. Uhlík, P. Košovan, Local pH and effective p KA of weak polyelectrolytes–insights from computer simulations. *Phys. Chem. Chem. Phys.* **2017**, *19*, 14376-14387.

36. J. Landsgesell, L. Nová, O. Rud, F. Uhlík, D. Sean, P. Hebbeker, C. Holm, P. Košovan, Simulations of ionization equilibria in weak polyelectrolyte solutions and gels. *Soft Matter* **2019**, *15*, 1155-1185.

37. A. Murmiliuk, P. Košovan, M. Janata, K. Procházka, F. Uhlík, M. Štěpánek, Local pH and Effective p K of a Polyelectrolyte Chain: Two Names for One Quantity? *ACS Macro Lett.* **2018**, *7*, 1243-1247.

38. M. Lund, B. Jönsson, Charge regulation in biomolecular solution. Quart. *Rev. Biophys.* **2013**, *46*, 265-281.

39. R. Arnold, The titration of polymeric acids. *J. Colloid Sci.* **1957**, *12*, 549-556.

40. O. Colombani, E. Lejeune, C. Charbonneau, C. Chassenieux, T. Nicolai, Ionization of amphiphilic acidic block copolymers. *J. Phys. Chem. B* **2012**, *116*, 7560-7565.

41. V.S. Rathee, H. Sidky, B.J. Sikora, J.K. Whitmer, Role of associative charging in the entropy–energy balance of polyelectrolyte complexes. *J. Am. Chem. Soc.* **2018**, *140*, 15319-15328.

42. J.L. Garcés, S. Madurga, C. Rey-Castro, F. Mas, Dealing with long-range interactions in the determination of polyelectrolyte ionization properties. Extension of the transfer matrix formalism to the full range of ionic strengths. *J. Polym. Sci. B* **2017**, *55*, 275-284.

43. R. Staňo, L. Nová, F. Uhlík, P. Košovan, Multivalent counterions accumulate in star-like polyelectrolytes and collapse the polymer in spite of increasing its ionization. *Soft Matter* **2020**, *16*, 1047-1055.

44. M. Stornes, P.M. Blanco, R.S. Dias, Polyelectrolyte-Nanoparticle mutual charge regulation and its influence on their complexation. *Colloids Surf. A* **2021**, *628*, 127258, 1-14.

45. C.F. Narambuena, P.M. Blanco, A. Rodriguez, D.E. Rodriguez, S. Madurga, J.L. Garcés, F. Mas, Non-monotonic behavior of weak-polyelectrolytes adsorption on a cationic surface: A Monte Carlo simulation study. *Polymer* **2021**, *212*, 123170, 1-10.

46. M.A. Hass, F.A. Mulder, Contemporary NMR studies of protein electrostatics. *Ann. Rev. Biophys.* **2015**, *44*, 53-75.

Supporting Information

Computational details and model parameters

The simulated system consisted of one dendrimer molecule fixed in the center of a cubic simulation box with edge length L = 42.3 nm. The dendrimer consisted of $G = 5$ generations of branches with $N = 6$ monomers per branch, resulting in the total number of 373 monomeric units. If we assume that one monomeric unit (bead) in the coarse-grained model represents one glucose unit, this setup corresponds to a glucose concentration of $c_{\mathrm{gluc}} = 1.50$ mg/mL. The melittin concentration is set to $c_{\mathrm{mel}} = 1.42$ mg/mL, corresponding to 22 molecules in the simulation box. The added salt concentration is fixed to $c_{\mathrm{cat}} = c_{\mathrm{an}} = c_{\mathrm{s}} = 20$ mM, corresponding to 911 pairs of small cations and anions in the simulation box. For simplicity, all particles (glycogen and melittin beads, small cations and anions) are represented by equal-sized spherical beads with the diameter of $\sigma = 0.35$ nm where σ is the parameter of the WCA potential (see Equation S1 below). All bonds in the glycogen and melittin molecules are set to equal bond length of $b = \sigma = 0.35$ nm and stiffness $k_{\mathrm{h}} = 100$ kT/σ^2.

Excluded volume interactions are applied for each pair of particles in the system (glycogen beads, melittin beads, small cations and anions). The steric interaction between particles *i* and *j* is modelled using the Weeks-Chandler-Andersen potential

$$U_{\mathrm{WCA}}(r_{ij}) = 4\varepsilon\left[\left(\frac{\sigma}{r_{ij}}\right)^{12} - \left(\frac{\sigma}{r_{ij}}\right)^{6} + \frac{1}{4}\right] H(2^{(1/6)}\sigma - r_{ij}) \qquad \text{(S1)}$$

where r_{ij} is the distance between the center of the particles *i* and *j*, ε is the depth of the potential well, σ defines the effective particle size and H(·) is the Heaviside step function. The connectivity between beads is maintained by a harmonic potential between each pair of bonded beads *i* and *j*, given by

$$U_{\mathrm{h}}(r_{ij}) = \frac{k_{\mathrm{h}}}{2}(r_{ij} - b)^2 \qquad \text{(S2)}$$

where k_h is the stiffness constant of the harmonic spring and $b = \sigma$ is the equilibrium bond length. The electrostatic interaction between charged particles *i* and *j* is given by the Coulomb potential:

$$U_{\mathrm{el}}(r_{ij}) = z_i z_j k_{\mathrm{B}} T \frac{l_{\mathrm{B}}}{r} \qquad \text{(S3)}$$

where $k_{\mathrm{B}}T$ is the thermal energy, z_i / z_j is the valency of bead *i* / *j* and l_{B} is the Bjerrum length. The electrostatic interactions were calculated using the P3M method, implemented in the ESPResSo simulation software.

The protonation states of the ionizable beads are sampled performing trial protonation/deprotonation moves using the constant pH algorithm.[S1] In these moves, the charge of the acidic/basic beads is switched following the reactions:

$$\mathrm{HA} \leftrightarrow \mathrm{A^-} + \mathrm{H^+} \qquad \text{(S4)}$$

$$\mathrm{BH^+} \leftrightarrow \mathrm{B} + \mathrm{H^+} \qquad \text{(S5)}$$

The equilibrium of these reactions was characterized by the acidity constant K_{A} of the acids HA and BH$^+$. These protonation/deprotonation trial moves are accepted with a probability given by

$$P^{\mathrm{acc}} = \min[1, \exp(-\beta\Delta U + \xi \ln(10)(\mathrm{pH} - \mathrm{p}K_{\mathrm{A},i}))] \qquad \text{(S6)}$$

where $\beta = 1/(k_{\mathrm{B}}T)$, $\mathrm{pH} = -\log_{10} a_{\mathrm{H}}$ and $\mathrm{p}K_{\mathrm{A},i} = -\log_{10} K_{\mathrm{A},i}$, where a_{H} is the activity of protons, $K_{\mathrm{A},i}$ is the acidity constant of the bead *i*, the extent of reaction ξ is +1 / -1 corresponds to the protonation/deprotonation step, $\Delta U = U_{\mathrm{n}} - U_{\mathrm{o}}$ is the difference between the energy in the new state U_{n}

and in the old state U_{o}. The electroneutrality of the system is kept by accordingly creating or removing a small cation particle.

Constant pH Monte Carlo simulations were performed using ESPResSo v4.1.4 software.[S2] Each simulation consisted of 10^5 equilibration cycles, followed by $2 \cdot 10^6$cycles during which the observables were sampled. One simulation cycle included 1000 steps of Langevin Dynamics (LD) integration, followed by $2N_{\mathrm{f}}$ Monte Carlo trial moves for sampling the N_{f} protonation/deprotonation reactions. At the end of each cycle, the observables were computed and saved for further processing. The LD was integrated using the Verlet algorithm with a time step of $\mathrm{d}t = 0.01\tau$, where $\tau = \sigma\sqrt{m/\varepsilon}$. The value of the particle mass *m* is arbitrary and does not affect the results. Temperature of the simulation is kept constant at $T = 300$ K using the Langevin thermostat with a damping constant $\gamma = 1.0\tau^{-1}$. The electrostatic interactions (Equation S1) were calculated using the P3M algorithm[S3] (tuned to ensure an accuracy of 10^{-3}) with the Bjerrum length $l_B = 0.71$nm (corresponding to water at $T = 300$ K). Periodic boundary conditions were applied in all directions of space.

Direct inputs of the simulations are the pH, the degree of substitution of glycogen (D_{s}) and the concentration of the species in solution. In return, the average charge *Z* of the species is measured as output. In addition, the radial distribution function $g(r)$ is computed as a function of the distance r to the central bead of glycogen (labeled as $G = 0$ in Fig. 1 in the main text).

The net charge *Z* of a molecule with *M* ionizable weak acid or base groups can be calculated from their degrees of ionization

$$Z = \sum_{i=1}^{M} z_i \alpha_i \qquad \text{(S7)}$$

where z_i is the charge of the group *i* in the ionized state; *i.e.* $z_i = -1$ for a monoprotic acid and $z_i = +1$ for a base. Under ideal conditions (*i.e.* in the absence of electrostatic interactions), the degree of ionization α_i^{ID} follows from the Henderson-Hasselbalch equation

$$\alpha_i^{\mathrm{ID}} = \frac{1}{1+10^{z_i(\mathrm{pH}-\mathrm{p}K_{\mathrm{a},i})}} \qquad \text{(S8)}$$

where $\mathrm{p}K_{\mathrm{a},i}$ is the equilibrium acidity constant of the group *i*. The non-ideal titration of polyelectrolytes typically differs from the Henderson-Hasselbalch equation.[S4-S9] This effect is often quantified by the effective $\mathrm{pK_a}$ of polyacids being higher than that of their parent monomers, whereas the opposite holds for polybases.

The local concentration $\mathrm{c_x}(r)$ of the molecule *x* (*x* = glycogen(glyc), melittin(mel), cation(cat), anion(an)) was determined as

$$c_x\,(r) = g_x\,(\mathrm{r})\langle c_x \rangle \qquad \text{(S9)}$$

where $\langle c_x \rangle$ and $g_x(r)$ are the analytical concentration and the radial distribution function of *x*.

Due to the strong electrostatic attraction between glycogen and melittin, $c_{\mathrm{mel}}(r)$ cannot be efficiently sampled directly. Therefore, we used the self-consistent histogram method by Ferrenberg and Swedsen.[S10,S11] In this method, a biasing potential

$$U_{\mathrm{bias}}\,(r) = \frac{k_{\mathrm{bias}}}{2}(\mathrm{r}-q)^2 \qquad \text{(S10)}$$

was applied between the central bead of glycogen and one melittin chain, restricting the two molecules into a certain umbrella window, defined by the force constant $k_{\mathrm{bias}} = 1\ k_B T/\ \sigma^2$, and the anchor point of the umbrella window, *q*, while and r is the instantaneous distance between the central beads of glycogen and the biased melittin chain. We carried out 30 simulations for *q* values ranging from $q = \sigma$ =0.36 nm to $q = L/2$ = 21 nm with increments of $\Delta q = \sigma$, providing us with an estimate of potential of mean force $PMF'(r)$.

The $PMF'(r)$ obtained from umbrella sampling is uniquely defined up to an additive constant which is determined by the absolute concentration of melittin

$$PMF(r) = PMF'(r) + K \qquad \text{(S11)}$$

To calculate $c_{mel}\ (r)$, the value of K must yield the total number of melittin chains in the integration volume

$$N_{\text{mel}} = \int_0^{d_{box}} c_{\text{mel}}(r) 4\pi r^2 dr = \int_0^{d_{box}} g(r)\langle c_{\text{mel}}\rangle 4\pi r^2 dr = \frac{N_{\text{mel}}}{L^3}\int_0^{R_{esf}} K g'(r) 4\pi r^2 dr \qquad \text{(S12)}$$

where $g'(r) = \exp\big(-\beta PMF'(r)\big) = K^{-1} g_{\text{mel}}(\text{r})$, $\langle c_{\text{mel}}\rangle = N_{mel}/L^3$ and $R_{esf} = L\sqrt[3]{3/4\pi}$ is the radius of a sphere with the same volume as the simulation box. However, from the simulation results is it possible to explicitly calculate $g(r)$ only for $r < L/2$. Therefore, we additionally assume that $g(r > L/2)$ is constant. With this assumption, we calculate *K* by rearranging Eq. S12, as

$$K^{-1} = \frac{1}{L^3}\int_0^{R_{esf}} 4\pi r^2 g'(r) dr \qquad \text{(S13)}$$

Once *K* is calculated, the absolute concentration, $c_{mel}\ (r)$, can be obtained as

$$c_{mel}\ (r) = \langle c_{mel}\rangle \exp\big(-\beta PMF(r)\big) = \langle c_{mel}\rangle g_{mel}(\text{r}) \qquad \text{(S14)}$$

It should be noted that the uncertainty in the value of K is the dominant contribution to uncertainty in the determined absolute concentration profiles of melittin.

The concentration of adsorbed melittin was obtained by integrating $c_{\text{mel}}(r)$ from the glycogen center to the adsorption threshold $r_{\text{ads}} = 6$ nm

$$c_{\text{ads}} = V_{\text{ads}}^{-1}\int_0^{r_{\text{ads}}} 4\pi \text{r}^2 c_{\text{mel}}(r) \text{dr} \qquad \text{(S12)}$$

where $V_{\text{ads}} = 4/3\pi r_{\text{ads}}^3$. The value of r_{ads} was selected arbitrarily based on the concentration profiles to delimit the dense core of the dendrimer. Note that the exact value of r_{ads} affects the magnitude of the computed partition coefficients but not the qualitative picture, how these partition coefficients vary with the pH or other parameters of the studied system. The concentration of free (non-adsorbed) melittin was estimated from the average concentration of melittin outside the adsorption threshold

$$c_{\text{free}} = V_{\text{free}}^{-1}\int_{r_{\text{ads}}}^{L/2} 4\pi \text{r}^2 c_{\text{mel}}(r)\ \text{dr} \qquad \text{(S13)}$$

where $V_{\text{free}} = 4/3\pi(L/2)^3 - V_{\text{ads}}$. Finally, the partition coefficient of melittin was calculated as

$$\log_{10} K = \log_{10}(c_{\text{ads}}/c_{\text{free}}) \qquad \text{(S14)}$$

Fourier-transformed infrared spectroscopy with attenuated total reflection (ATR-FTIR)

To confirm the structure of modified glycogen and 9,10-dihydroanthracene-9,10-α,β-succinic anhydride (DASA), the ATR-FTIR was used. The spectra are presented in Figure S1 and were interpreted as follows:

DASA: ν(C_6H_4) = 1860 cm^{-1}, ν(C=O) = 1780 cm^{-1}, ν(aromatic ring) = 1460 cm^{-1}, ν_a(C-O-C) = 1230, 1210, and 1070 cm^{-1}, ν(anhydride ring) = 970, 920, and 900 cm^{-1}, δ(C-H) = 755, 700, and 635 cm^{-1}.

Unmodified GG: ν(O-H) = 3300 cm^{-1}, $\nu_a(CH_2)$ = 2930 cm^{-1}, δ(NH_2) = 1630 cm^{-1}, δ(O-H) = 1450-1330 cm^{-1}, ν_a(C-O-C) = 1150 cm^{-1}, ν(C-OH) = 1080 cm^{-1}, ν(ring) = 1010 cm^{-1}, ν(C-C) = 930 cm^{-1}, δ(C-H) = 850, 760, and 705 cm^{-1}.

GGS6: ν(O-H) = 3300 cm^{-1}, $\nu_a(CH_2)$ = 2930 cm^{-1}, ν(C=O) = 1730 cm^{-1}, $\delta(NH_2)$ = 1570 cm^{-1}, δ(O-H) = 1400-1320 cm^{-1}, ν_a(C-O-C) = 1260, 1205, 1150 cm^{-1}, ν(C-OH) = 1080 cm^{-1}, ν(ring) = 1015 cm^{-1}, ν(C-C) = 940 cm^{-1}, δ(C-H) = 870, 760, 710, and 655 cm^{-1}.

GGP6: ν(O-H) = 3300 cm^{-1}, $\nu_a(CH_2)$ = 2930 cm^{-1}, ν(C=O) = 1720 cm^{-1}, $\delta(NH_2)$ = 1585-1565 cm^{-1}, ν(aromatic ring) = 1485-1445 cm^{-1}, δ(O-H) = 1385 cm^{-1}, ν_a(C-O-C) = 1280, 1255, 1150 cm^{-1}, ν(C-OH) = 1080 cm^{-1}, ν(glucose ring) = 1020 cm^{-1}, δ(C-C) = 935 cm^{-1}, δ(C-H) = 840, 750, 710, and 650 cm^{-1}.

GGC6: ν(O-H) = 3300 cm^{-1}, $\nu_a(CH_2)$ = 2930 cm^{-1}, ν(C=O) = 1725 cm^{-1}, $\delta(NH_2)$ = 1560 cm^{-1}, $\delta(CH_2)$ = 1445-1400 cm^{-1}, ν_a(C-O-C) = 1150 cm^{-1}, ν(C-OH) = 1080 cm^{-1}, ν(glucose ring) = 1025 cm^{-1}, δ(C-C) = 935 cm^{-1}, δ(C-H) = 840, 760, and 705 cm^{-1}.

GGA6: the spectrum is almost identical to that of pure GG due to the low degree of hydroxyl substitution with highly hydrophobic DASA residues.

Solution-state ^{1}H nuclear magnetic resonance (NMR) spectroscopy

Proton NMR spectroscopy was used to confirm the chemical composition and structure of modified GG. The measurements were carried out under RT, at 400 MHz using THF-d_8 or D_2O as a solvent for DASA or for the modified GG samples, respectively. ^{1}H NMR spectra are presented in Figure S2 and were interpreted as follows:

Unmodified GG: δ 5.44 (br s, 1H), 4.00-3.30 (br m, 3.73H), 2.45-2.37 (m, 0.17H), 2.18-2.05 (m, 0.23H), 1.50 (d, 0.09H), 1.20 (t, 0.08H).

GGA6: δ 7.40 (d, 0.15H), 7.20 (br, 0.14H), 5.43 (br s, 1H), 4.63 (s, 0.18H), 4.00-3.38 (br m, 5.04H), 3.14 (s, 0.21H), 2.76 (s, 0.06H), 1.33-1.20 (m, 0.05H).

GGC6: δ 8.10 (d, 0.02H), 6.90 (d, 0.02H), 5.40 (br s, 1H), 4.00-3.45 (br m, 5.15H), 3.37 (s, 0.21H), 3.25-3.20 (q, 0.69H), 3.00-2.60 (br m, 1.14H), 1.95 (br s, 0.77H), 1.78 (br s, 1H), 1.44 (br s, 0.95H), 1.30 (dd, 0.92H).

GGP6: δ 7.87-7.40 (br m, 1.47H), 6.50 (d, 0.06H), 5.40 (br s, 1H), 4.00-3.45 (br m, 4.73H), 3.37 (s, 0.16H), 3.00 (q, 0.49H), 2.96 (s, 0.08H), 2.70 (s, 0.22H), 1.30 (t, 0.03H), 1.14 (dd, 0.54H), 1.00 (t, 0.02H).

GGS6: δ 8.10 (d, 0.02H), 6.90 (d, 0.02H), 5.60-5.40 (br m, 1H), 4.00-3.87 (br m, 1.96H), 3.73 (s, 0.32H), 3.37 (s, 0.12H), 3.25-3.20 (q, 0.69H), 2.69 (br s, 1.27H), 2.53 (br s, 1.7H), 2.42 (s, 0.2H), 1.40 (t, 0.05H), 1.33 (dd, 0.73H), 1.15 (t, 0.04H).

Characterization of modified glycogens

Contents of carbon, hydrogen, and sodium in the samples of modified glycogen (GG) were determined by elemental analysis in order to confirm their composition. Theoretical contents of these elements in modified GG were calculated from the known loads of reagents assuming their complete conversion into product and presented in Table S1 together with experimental values.

To evaluate the colloidal properties of modified glycogens, dependencies of their hydrodynamic radius and ζ-potential on temperature or pH were determined by means of dynamic light scattering. The samples were dissolved in phosphate buffered saline (PBS) or citrate-phosphate buffer for the registration of temperature and pH dependencies, respectively (Figures S3, S4).

Table S1. Properties of modified glycogen samples.

Sample	Theoretical content[a]			Experimental content[b]		
	C, wt.%	H, wt.%	Na, wt.%	C, wt.%	H, wt.%	Na, wt.%
GGS3	45.3	5.7	5.3	40.3	5.9	4.2
GGS6	45.8	5.4	8.6	39.7	5.6	6.4
GGP3	49.2	5.4	3.6	41	5.9	2
GGP6	52.1	4.9	5.8	42.4	5.9	3.1
GGC3	48.6	6.2	3.4	41.4	6.4	1.4
GGC6	51.2	6.3	5.6	42.7	6.8	2.9
GGA3	52.2	5.8	1.9	40.9	6.5	0.2
GGA6	57.1	5.5	3.1	41.5	6.0	0.5

[a] calculated from the composition of reaction mixture; [b] determined by elemental analysis

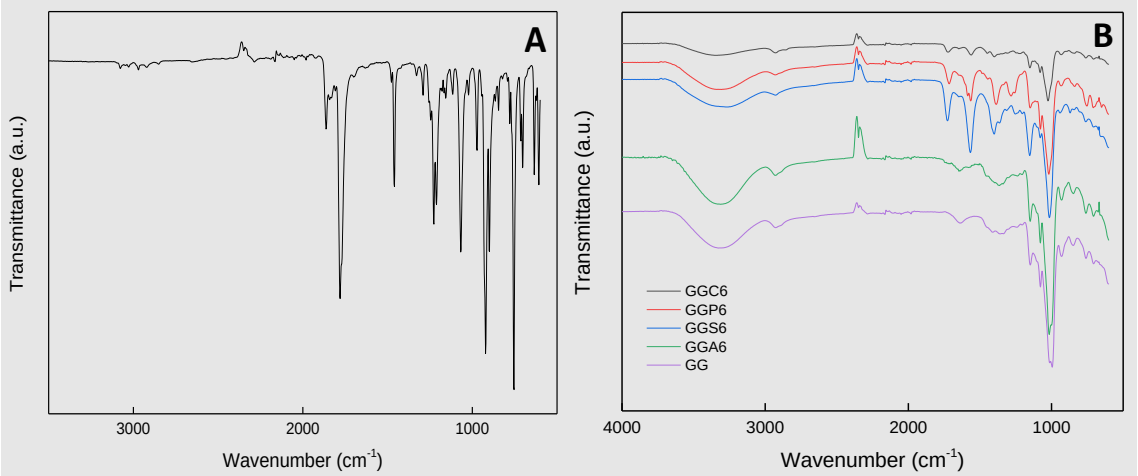

Figure S1. (A) ATR-FTIR spectrum of 9,10-dihydroanthracene-9,10-α,β-succinic anhydride; (B) FTIR spectra of glycogen and its derivatives.

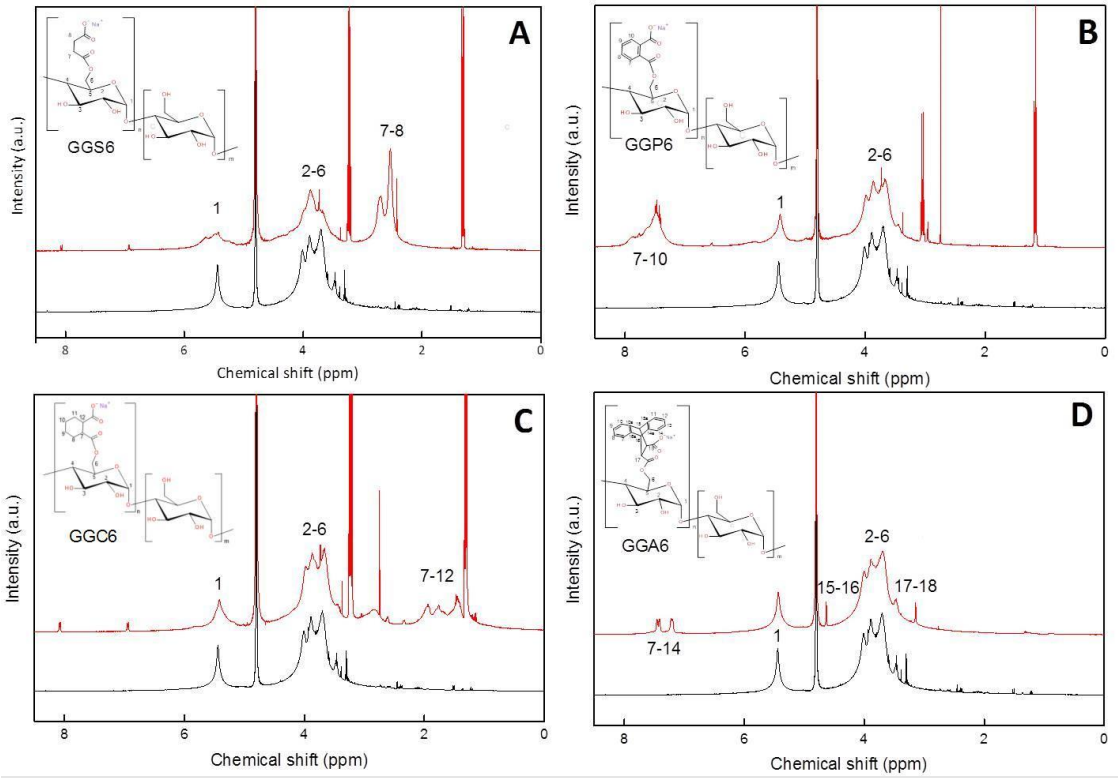

Figure S2. ^{1}H NMR spectra of glycogen (black) and its derivatives (red). A, B, C, and D are the spectra of glycogen succinate, phthalate, cyclohexanedicarboxylate, and dihydroanthracene-succinate, respectively.

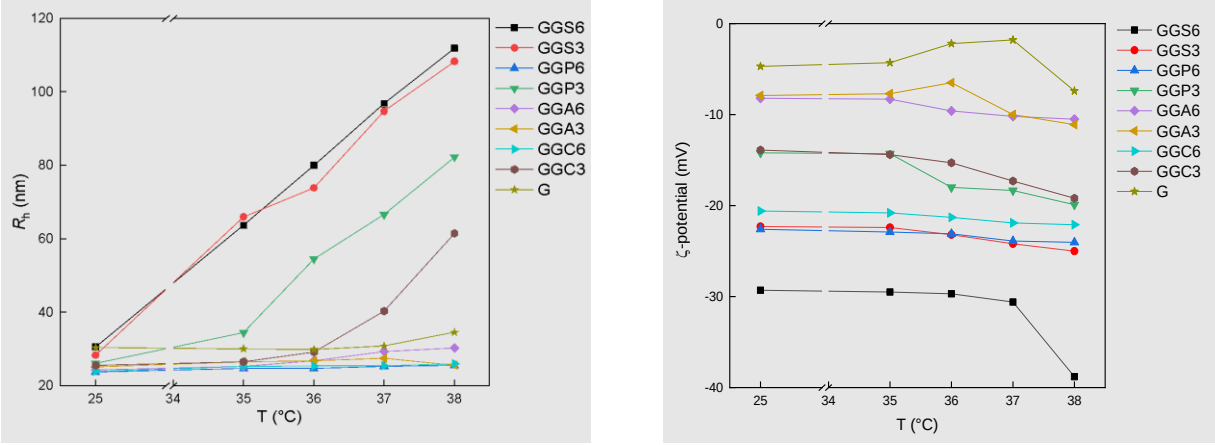

Figure S3. Temperature dependence of hydrodynamic radius and ζ-potential of pure and modified glycogen samples in PBS.

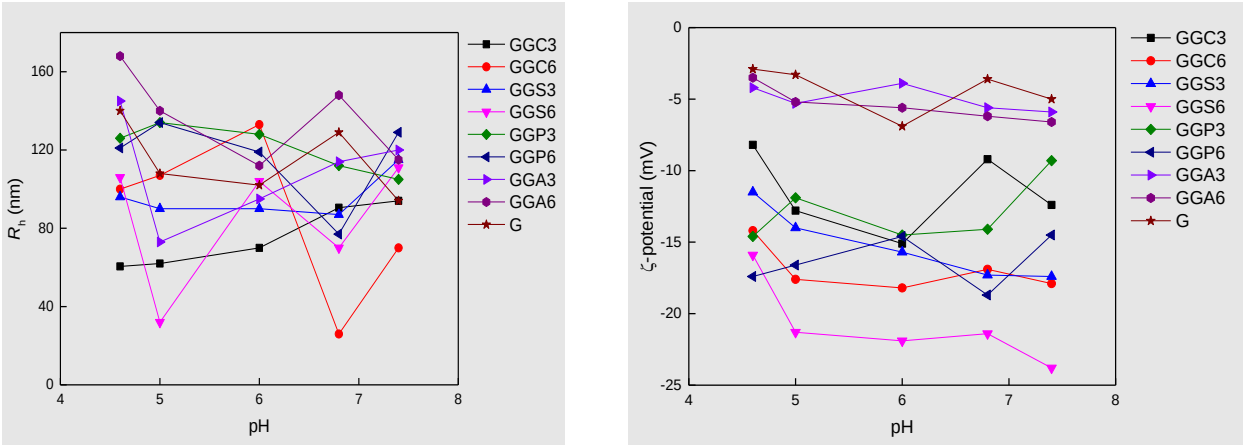

Figure S4. pH dependence of hydrodynamic radius and ζ-potential of pure and modified glycogen samples in citrate-phosphate buffer.

Table S2. Hemolysis of only modified glycogens without melittin.

	hemolysis				total	
	a	b	c	d	diameter	SD
1%Triton	100.0	100.0	100.0	100.0	100.0	0.0
Melittin 4,5 μg/ml		71.1	73.3	75.3	73.2	2.1
glycogen 2 mg/ml + 4,5 μg/ml melittin		50.3	76.8	70.8	66.0	13.9
glycogen 2 mg/ml	0.8	0.9	2.1	0.7	1.2	0.6
GGS3 2 mg/ml	-0.5	0.0	0.5		0.0	0.5
GGS6 2 mg/ml		1.2	0.3	0.4	0.6	0.5
GGP3 2 mg/ml	1.2	0.1	0.5		0.6	0.5
GGP6 2 mg/ml		0.0	-0.6	0.6	0.0	0.6
GGC3 2 mg/ml	-0.5	-0.2	0.8		0.0	0.7
GGC6 2 mg/ml		-0.1	-0.6	-0.1	-0.3	0.3
GGA3 2 mg/ml	0.8	-0.1	0.6		0.5	0.5
GGA6 2 mg/ml		-0.1	0.0	0.4	0.1	0.3
PBS	0.0	0.0	0.0	0.0	0.0	0.0

Concentration profile from molecular simulations of glycogen with D_s = 0.25

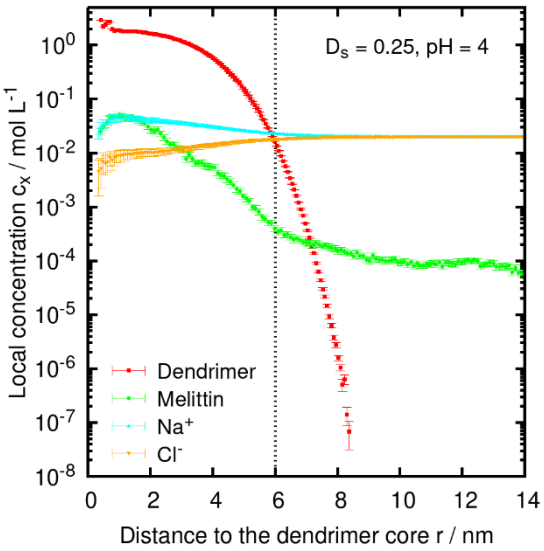

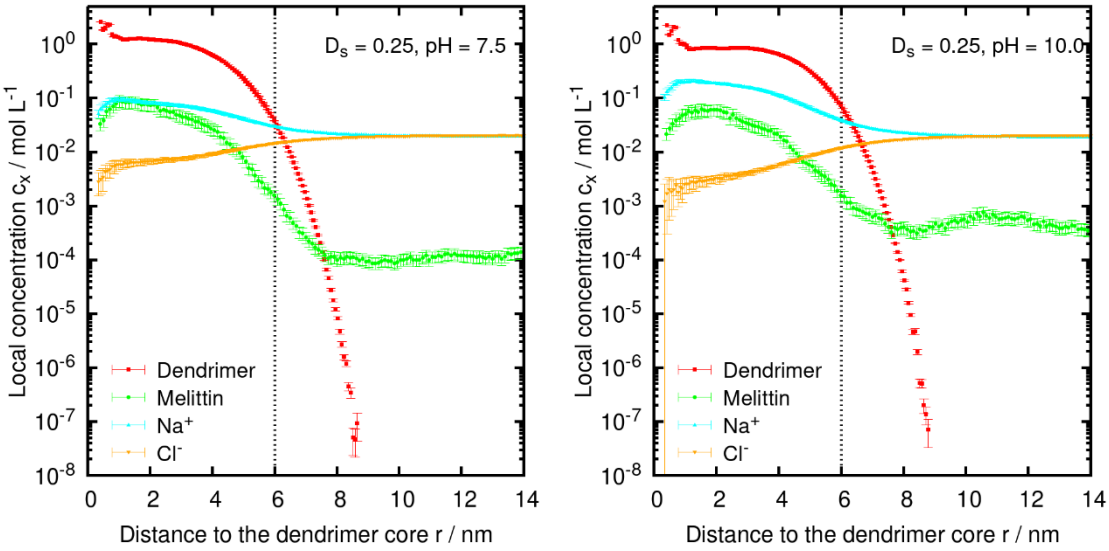

Fig. S5 Concentration profiles of various ionic species, plotted as a function of distance from the core of the dendrimer r. The results correspond to the degree of substitution of glycogen D_s = 0.25 and the following pH values: 4.0, 7.5 and 10.0. The vertical dashed line at r = 6nm denotes the boundary between interior and exterior of the dendrimer, used for the calculation of adsorption coefficient.

Dynamic light scattering (DLS) and Zeta potential measurements. The routine measurements of modified glycogens and melittin solutions revealing the temperature and pH trends of their intensity-weighted hydrodynamic radius (R_H) and Zeta potential (ξ) were carried out on a Zetasizer NanoZS instrument, model ZEN3600 (Malvern Instruments, Malvern, UK). The concentration of measured solutions was 0.72 mg/ml. The temperature was kept at 25 °C (± 0.1°C). The titration experiments were performed using the same instrument connected to the autotitrator MPT-2 (Malvern Instruments, Malvern, UK). R_H was measured at a scattering angle of θ = 173°, and the data were processed with the Repes algorithm.[S12] The data of zeta potential were evaluated using the model of Smoluchowski. The concentration of titrant (HCl) was 3mol/L and concentrations of polymer solutions were 0.1 mg/ml in MilliQ water for pH titrations. In the study of glycogen-melittin interaction, a solution of glycogen at concentration of 0.1 mg/ml was titrated by melittin solution at concentration of 1.4 mg/ml. The solutions were prepared in citric acid phosphate buffer solution at pH 5.0, 6.0 and 7.4, and filtered before measurement using a 0.46 μm PVDF syringe filter. Volume of polymer solution was 5 ml, volume of each injection varied depending on pH of solutions from 100 to 150 μL. Each step of the autotitration includes injection of titrant, circulation and stirring process for 20 minutes, and equilibration of the sample for 10 minutes. The measurements were performed at 25°C (± 0.1°C).

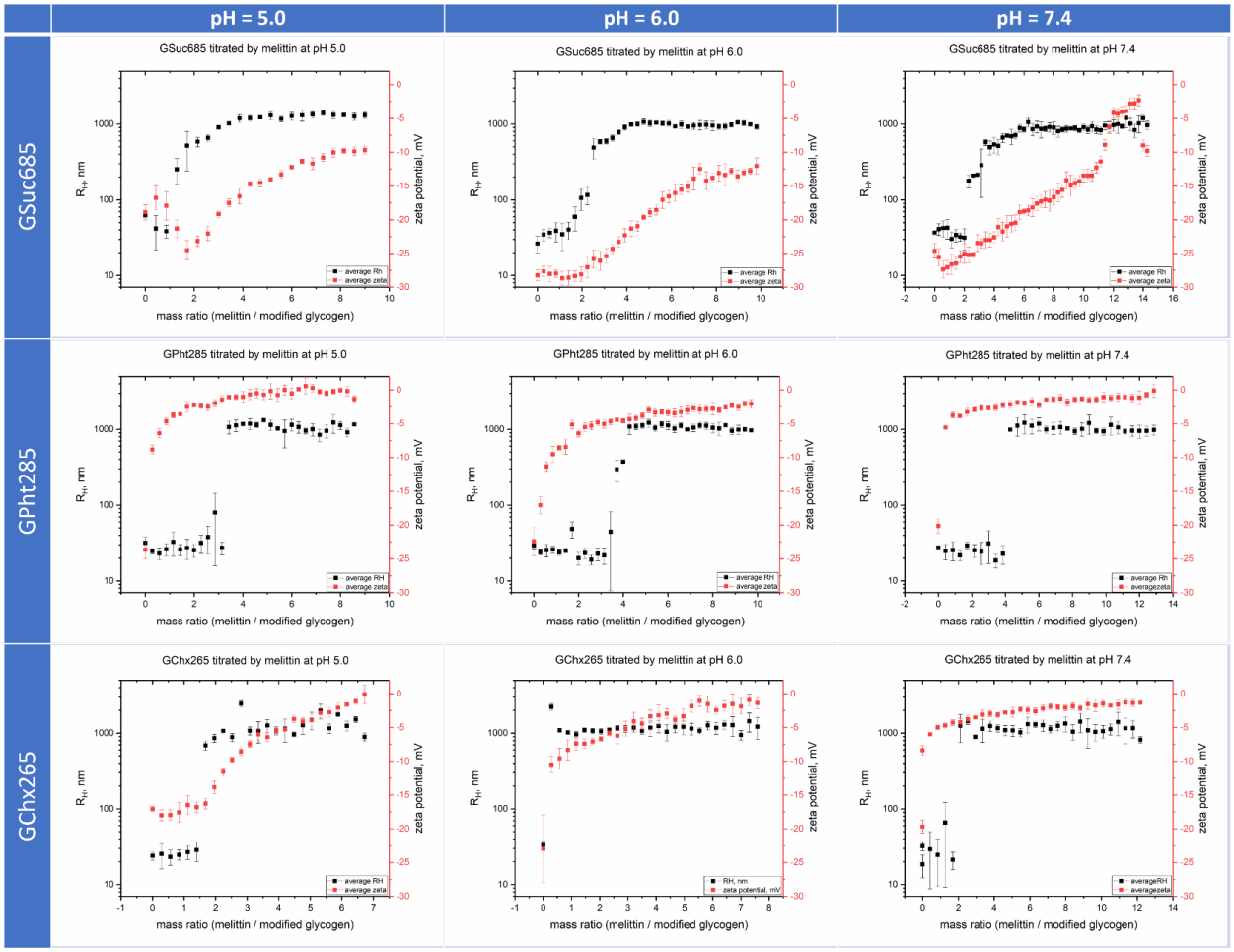

Figure S6. DLS titration and electrophoresis of different functionalized glycogen samples ($c_{\mathrm{glyc}} = 0.1$ mg/mL) with melittin ($c_{\mathrm{mel}} = 1.4$ mg/mL) at pH values of 5.0, 6.0 and 7.4.

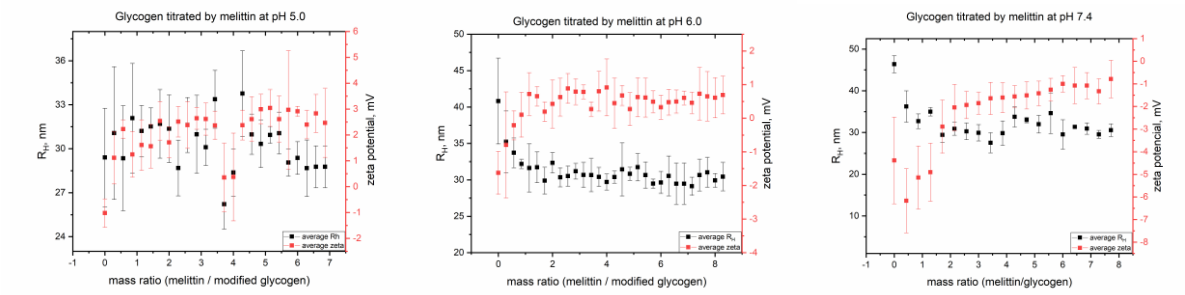

Figure S7. Control experiments to Fig.S6 - DLS tittrations of unmodified glycogen with melittin.

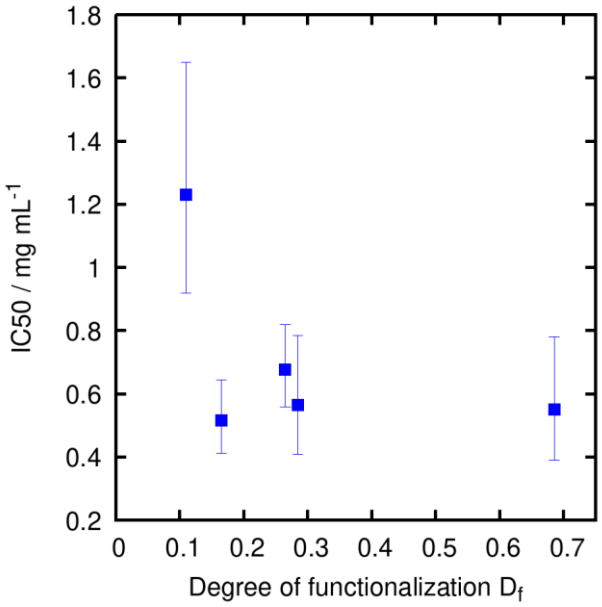

Figure S8. Effective concentrations based on the carboxyl group functionality. Error bars indicate 95% confidence interval.

REFERENCES

S1. C. E. Reed and W. F. Reed, Monte Carlo study of titration of linear polyelectrolytes. *The Journal of chemical physics* **1992**, *96*, 1609-1620.

S2. F. Weik, R. Weeber, K. Szuttor, K. Breitsprecher, J. de Graaf, M. Kuron, and C. Holm, ESPResSo 4.0–an extensible software package for simulating soft matter systems. *The European Physical Journal Special Topics* **2019**, *227*, 1789-1816.

S3. R. W. Hockney, J. W. Eastwood, Semiconductor device simulation. Computer simulation using particles, IOP, Bristol, 1988.

S4. L. Nová, F. Uhlík, P. Košovan, Local pH and effective pKa of weak polyelectrolytes–insights from computer simulations. *Physical Chemistry Chemical Physics* **2017**, *19*, 14376-14387.

S5. J. Landsgesell, L. Nová, O. Rud, F. Uhlík, D. Sean, P. Hebbeker, and P. Košovan, Simulations of ionization equilibria in weak polyelectrolyte solutions and gels. *Soft Matter* **2019**, *15*, 1155-1185.

S6. A. Murmiliuk, P Košovan, M. Janata, K. Procházka, F. Uhlík, and M. Štěpánek, Local pH and Effective pK of a Polyelectrolyte Chain: Two Names for One Quantity? *ACS Macro Letters* **2018**, *7*, 1243-1247.

S7. M. Lund and B. Jönsson, Charge regulation in biomolecular solution. *Quarterly reviews of biophysics* **2013**, *46*, 265-281.

S8. R. Arnold, The titration of polymeric acids. *Journal of Colloid Science* **1957**, *12*, 549-556.

S9. O. Colombani, E. Lejeune, C. Charbonneau, C. Chassenieux, and T. Nicolai, Ionization of amphiphilic acidic block copolymers. *The Journal of Physical Chemistry B* **2012**, *116*, 7560-7565.

S10. A. M. Ferrenberg and R. H. Swendsen, New Monte Carlo Technique for Studying Phase Transitions. *Physical Review Letters* **1989**, *63*, 1658-1658.

S11. D. Frenkel, B. Smit, Understanding Molecular Simulation: from Algorithms to Applications. Academic Press, Waltham, MA, 2001.

S12. J. Jakeš, Regularized Positive Exponential Sum (REPES) Program - A Way of Inverting Laplace Transform Data Obtained by Dynamic Light Scattering. *Collection of Czechoslovak Chemical Communications* **1995**, *60*, 1781-1797.